Unique foot posture in Neanderthals reflects their body mass and high mechanical stress

Rita Sorrentino [a, b, *], Nicholas B. Stephens [c, *], Damiano Marchi [d, e], Lily J.D. DeMars [c],
Carla Figus [b], Eugenio Bortolini [b], Federica Badino [b, f], Jaap P.P. Saers [g], Matteo Bettuzzi [h],
Francesco Boschin [i], Giulia Capecchi [i], Francesco Feletti [j], Tiziana Guarnieri [a, k],
Hila May [l, m], Maria Pia Morigi [h], William Parr [n], Stefano Ricci [i], Annamaria Ronchitelli [i],
Jay T. Stock [g, o, p], Kristian J. Carlson [e, q], Timothy M. Ryan [c], Maria Giovanna Belcastro [a],
Stefano Benazzi [b, r]

[a] Department of Biological, Geological and Environmental Sciences, University of Bologna, Bologna 40126, Italy
[b] Department of Cultural Heritage, University of Bologna, Ravenna 48121, Italy
[c] Department of Anthropology, The Pennsylvania State University, State College, PA 16802, USA
[d] Department of Biology, University of Pisa, Pisa 56126, Italy
[e] Evolutionary Studies Institute, University of the Witwatersrand, Palaeosciences Centre, Johannesburg, Wits 2050, South Africa
[f] Research Group on Vegetation, Climate and Human Stratigraphy, Lab. of Palynology and Palaeoecology, CNR - Institute of Environmental Geology and
Geoengineering (IGAG), Milan 20126, Italy
[g] Department of Archaeology, Cambridge University, Cambridge CB2 3EX, UK
[h] Department of Physics and Astronomy, University of Bologna, Bologna 40127, Italy
[i] U.R. Preistoria e Antropologia, Dipartimento di Scienze Fisiche, della Terra e dell'Ambiente, Università degli Studi di Siena, Siena 53100, Italy
[j] Department of Diagnostic Imaging, Ausl Romagna, S.Maria delle Croci Hospital, Ravenna 48121, Italy
[k] Interuniversity Consortium "Istituto Nazionale Biostrutture e Biosistemi" (INBB-Biostructures and Biosystems National Institute), Rome 00136, Italy
[l] Department of Anatomy and Anthropology, Sackler Faculty of Medicine, Tel Aviv University, Tel Aviv 39040, Israel
[m] The Shmunis Family Anthropology Institute, The Dan David Center for Human Evolution and Biohistory Research, Sackler Faculty of Medicine, Tel Aviv
University, Tel Aviv 39040, Israel
[n] Surgical and Orthopaedic Research Laboratories, Prince of Wales Hospital, University of New South Wales, Sydney 1466, Australia
[o] Department of Anthropology, Western University, London, Ontario N6A 3K7, Canada
[p] Department of Archaeology, Max Planck Institute for the Science of Human History, Jena 07745, Germany
[q] Department of Integrative Anatomical Sciences, Keck School of Medicine, University of Southern California, Los Angeles 90089, California, USA
[r] Department of Human Evolution, Max Planck Institute for Evolutionary Anthropology, Leipzig 04103, Germany

ARTICLE INFO

ABSTRACT

Neanderthal foot bone proportions and morphology are mostly indistinguishable from those of *Homo sapiens*, with the exception of several distinct Neanderthal features in the talus. The biomechanical implications of these distinct talar features remain contentious, fueling debate around the adaptive meaning of this distinctiveness. With the aim of clarifying this controversy, we test phylogenetic and behavioral factors as possible contributors, comparing tali of 10 Neanderthals and 81 *H. sapiens* (Upper Paleolithic and Holocene hunter-gatherers, agriculturalists, and postindustrial group) along with the Clark Howell talus (Omo, Ethiopia). Variation in external talar structures was assessed through geometric morphometric methods, while bone volume fraction and degree of anisotropy were quantified in a subsample ($n = 45$). Finally, covariation between point clouds of site-specific trabecular variables and surface landmark coordinates was assessed. Our results show that although Neanderthal talar external and internal morphologies were distinct from those of *H. sapiens* groups, shape did not significantly covary with either bone volume fraction or degree of anisotropy, suggesting limited covariation between external and internal talar structures. Neanderthal external talar morphology reflects ancestral retentions, along with various adaptations to high levels of mobility correlated to their presumably unshod hunter-gatherer lifestyle. This pairs with their high site-specific trabecular bone volume fraction and anisotropy, suggesting intense and consistently oriented locomotor loading, respectively. Relative to

* Corresponding authors.
E-mail addresses: rita.sorrentino2@unibo.it (R. Sorrentino), nbs49@psu.edu (N.B. Stephens).

*H.*sapiens, Neanderthals exhibit differences in the talocrural joint that are potentially attributable to cultural and locomotor behavior dissimilarity, a talonavicular joint that mixes ancestral and functional traits, and a derived subtalar joint that suggests a predisposition for a pronated foot during stance phase. Overall, Neanderthal talar variation is attributable to mobility strategy and phylogenesis, while *H. sapiens* talar variation results from the same factors plus footwear. Our results suggest that greater Neanderthal body mass and/or higher mechanical stress uniquely led to their habitually pronated foot posture.

1. Introduction

Neanderthals (*Homo neanderthalensis*) are phylogenetically regarded as a sister species to *Homo sapiens*, and when their cranial and postcranial anatomy are compared, there is a suite of morphological features that distinguish their form from Pleistocene and recent *H. sapiens* (Harvati, 2010). Generally, Neanderthal cranial morphology is characterized by a long vault, marked occipital bun, pronounced brow ridges, midfacial prognathism, and a wide nasal aperture (Trinkaus, 2006; Weaver et al., 2007; Weaver, 2009; Benazzi et al., 2015; Wroe et al., 2018). Postcranially, Neanderthals are robust, with a wide pelvis, a mediolaterally broad chest, short legs, and rugose muscle attachments (Trinkaus et al., 1991; Steudel-Numbers and Tilkens, 2004; García-Martínez et al., 2018; Belcastro et al., 2020). Taken together, these features are often attributed to genetic drift, stemming from a low effective population size, along with body proportions that are functional adaptations to cyclic Pleistocene glaciations and ambush hunting subsistence strategies (Pearson, 2000; Weaver, 2009). While it is certain that many skeletal features are explained via interactions between drift and functional adaptations to cold, many may also represent plastic responses during life related to behaviorally driven repetitive mechanical loading, such as that occurs during locomotion (Trinkaus et al., 1991).

Similar to *H. sapiens,* Neanderthals were fully bipedal (Harcourt-Smith, 2004), but their comparatively robust skeletons and variations in cross-sectional geometry and muscle attachments of their lower limbs have led researchers to suggest that there were meaningful differences from the former in levels of biomechanical stress and habitual movements (e.g., more mediolateral stress on lower limbs in the latter; Trinkaus et al., 1991; Pearson, 2000; Belcastro et al., 2020). Understanding these morphofunctional differences will help clarify how Pleistocene *H. sapiens* morphology evolved in response to changes in environment, behavior, and culture. Comparative studies of hominoid foot bones can deepen our understanding of the hominin transition to obligate bipedalism (Marchi, 2010; Prang, 2015; Holowka et al., 2017; Fernández et al., 2018; Holowka and Lieberman, 2018; DeSilva et al., 2019; Sorrentino et al., 2020a) and provide an interpretive framework for exploring functional responses to the myriad cultural innovations from the Pleistocene to today (Trinkaus, 2005; Zipfel and Berger, 2007; Baxter et al., 2012; Holowka et al., 2018).

Pleistocene *H. sapiens* and Neanderthals share foot proportions, morphology indicative of longitudinal and transverse arches, and a fully adducted hallux (Trinkaus, 1983; Trinkaus et al., 1991). Neanderthals differ from *H. sapiens*, however, in having more robust tarsals, metatarsals, and proximal phalanges, as demonstrated by their enlarged articular surfaces, stronger diaphyses, and higher rugosity of entheses, which are suggestive of adaptations to increased locomotor loading (Trinkaus, 1983; DeSilva et al., 2019; Pablos et al., 2019).

Within the foot, the talus has been the subject of many comparative studies that have helped to increase our knowledge on the evolution of bipedalism (Latimer et al., 1987; Harcourt-Smith, 2004; Parr et al., 2011, 2014; Prang, 2015, 2016; Turley et al., 2015; Su and Carlson, 2017; Sorrentino et al., 2020a), as well as the behavioral and cultural factors influencing modern human variation in talar morphology (Turley et al., 2015; Saers et al., 2018, 2019; Sorrentino et al., 2020b, c). Furthermore, talar variation is better understood because of the comparatively high number of well-preserved fossils, with the talus being one of the most commonly recovered pedal elements in the fossil record (Pablos, 2015). Therefore, the talus is an optimal target for inferring what—if any—habitual locomotor differences may have existed between *H. sapiens* and Neanderthals (Rhoads and Trinkaus, 1977; Trinkaus, 1983; Rosas et al., 2017; Pablos et al., 2019; Pearson et al., 2020).

The talus couples the tibia and fibula at the talocrural joint via the trochlea and medial and lateral malleolar surfaces. The talus also articulates with the calcaneus and navicular via the subtalar (posterior, medial, and anterior calcaneal facets) and transverse tarsal (navicular facet) joints. Without direct muscle attachments, all motion of the talus during movement of the foot is constrained by ligaments as force is transmitted through the articular surfaces (Aiello and Dean, 1990; Huson, 1991; Parr et al., 2014; Griffin et al., 2015).

Neanderthal tali differ externally from *H. sapiens* tali by exhibiting a relatively larger trochlea, more concave medial and lateral malleolar facets, a mediolaterally broader talar head, and a shorter neck (Rhoads and Trinkaus, 1977; Trinkaus, 1983; Lu et al., 2011; Boyle and DeSilva, 2015; Pablos, 2015; Pablos et al., 2017, 2019; Pearson et al., 2020; Rosas et al., 2017). Among the unique Neanderthal talar traits, the broad talocrural articular surface is purportedly an adaptation to high levels of activity and biomechanical stress (Rhoads and Trinkaus, 1977), or, instead, increased body mass (Rosas et al., 2017). Body mass has been suggested to influence the Neanderthal lateral malleolar expansion and projection (Rosas et al., 2017), even if have associated this feature with talocrural reinforcement against lateral loading. While mediolateral enlargement of the talar head is common in some Middle Pleistocene hominins, suggesting ancestry of this trait (Pearson et al., 2008; Lu et al., 2011), Rosas et al. (2017) have found no correlation between talar head and body size, suggesting that a broad talar head (primarily observed in dorsal view) is an anatomical and/or functional Neanderthal specialization. The Neanderthal talar neck is particularly short in respect to its elongated talar body, and Rhoads and Trinkaus (1977) highlighted an inverse relationship between the length of the neck and the trochlea as associated with increased body mass in Neanderthals. However, recently, it has been suggested that the length of the talar neck is independent of talar body length (Rosas et al., 2017). Generally, a short talar neck is a common feature of all *Homo* fossils except modern humans, and thus, it could represent a primitive trait (Pablos, 2015).

Ultimately, there is no consensus on whether Neanderthal talar traits are ancestral retentions, secondary expressions of their robust postcranial skeleton, or plastic features related to selective pressures from high levels of behaviorally driven mechanical stress (Rhoads and Trinkaus, 1977; Trinkaus, 1983; Aiello and Dean, 1990;

Lu et al., 2011; Boyle and DeSilva, 2015; Pablos, 2015; Pablos et al., 2017, 2019; Rosas et al., 2017; Pearson et al., 2020). Here we investigate the distinctiveness of 10 Neanderthal tali in comparison with those of *H. sapiens* (i.e., the Clark Howell talus from Omo, Upper Paleolithic and Holocene hunter-gatherer, agriculturalist, and postindustrial groups; Table 1 and Supplementary Online Material [SOM] Fig. S1) representing diverse subsistence and mobility strategies (Turley et al., 2015; Saers et al., 2018; Sorrentino et al., 2020b). Our analysis utilized (semi)landmark-based geometric morphometric methods to quantify complete external talar morphology along with configurations of isolated articular facets (Sorrentino et al., 2020a). Additionally, trabecular bone properties from a subsample of these tali were quantified, and site-specific bone volume fraction (BV/TV) and degree of anisotropy (DA) were statistically compared to provide insight into potential biomechanical differences (Kivell, 2016; Stephens et al., 2018). Because external form and internal bone respond to functional demands (Lieberman et al., 2001; Ruff et al., 2012; Kivell, 2016), we performed a covariation analysis between landmark coordinates and point clouds of site-specific trabecular variables to assess similar or different responses to the mechanical environment characterizing both taxa.

Our predictions are based on inferred variation in subsistence and mobility strategies, with the expectation that talar external morphology plastically responds to differences in loading regime, activity level, and footwear use as these factors contribute to structural change of bones (Hoffmann, 1905; Barnett, 1962; Trinkaus, 2005; Carlson et al., 2007; Zipfel and Berger, 2007; D'Août et al., 2009). Levels of mobility are strongly associated with mechanical loading and morphological variation of the lower limb bones (Carlson and Marchi, 2014). The term 'mobility' may be defined differently, for example, to refer to greater range of motion (e.g., greater joint mobility). Here, 'mobility' invokes locomotion (e.g., distance traveled) as a separate concept from levels of physical activity. For instance, high mobility can characterize agriculturalists who may have exhibited high residential mobility (e.g., regularly moved camps between fields), or, alternatively, low-mobility agriculturalists may still experience substantial physical activities if they are practicing particularly intensive farming/food processing activities (Carlson and Marchi, 2014). Comparative studies have shown that talar shape of highly mobile (i.e., high levels of distance traveled) unshod hunter-gatherers consists of a more dorsally convex talar corpora, a more laterally projected fibular malleolar facet, a more cupped medial malleolar facet, a relatively short talar

Table 1
Sample examined in the present study.

Sample	Time period	Recovery location	Subsistence	Mobility	Footwear
Clark Howell talus (*n* = 1)	Middle Stone Age[a] (~104−196 ka)	Omo, Ethiopia	Hunter-gatherer	High+	Unshod/soft covering
Neanderthals (*n* = 10)					
Krapina 237	130 ± 10 ka[b]	Croatia	Hunter-gatherer	High+	Unshod/soft covering
Krapina 235	130 ± 10 ka[b]	Croatia	Hunter-gatherer	High+	Unshod/soft covering
Tabun C1	122 ± 16 ka[c]	Israel	Hunter-gatherer	High+	Unshod/soft covering
Regourdou 1	70−56 ka[d]	France	Hunter-gatherer	High+	Unshod/soft covering
Amud 1	53 ± 8 ka[e]	Israel	Hunter-gatherer	High+	Unshod/soft covering
Shanidar 5	ca. 55−45 ka[f]	Iraq	Hunter-gatherer	High+	Unshod/soft covering
La Ferrassie 1	54−40 ka[g]	France	Hunter-gatherer	High+	Unshod/soft covering
La Ferrassie 2	54−40 ka[g]	France	Hunter-gatherer	High+	Unshod/soft covering
La Chapelle	47−56 ka[h]	France	Hunter-gatherer	High+	Unshod/soft covering
Spy 2 (SP4B)	36 ka[i] BP	Belgium	Hunter-gatherer	High+	Unshod/soft covering
Upper Paleolithic hunter-gatherers (*n* = 7)					
Paglicci 25	Gravettian[j] (29−27 ka cal. BP)	Italy	Hunter-gatherer	High+	Unshod/soft covering
Veneri 2	Gravettian[k] (25 ka cal. BP)	Italy	Hunter-gatherer	High+	Unshod/soft covering
Villabruna	Epigravettian[l] (14 ka cal. BP)	Italy	Hunter-gatherer	High	Unshod/soft covering
Romito 7	Epigravettian[m] (ca.14 ka cal. BP)	Italy	Hunter-gatherer	High	Unshod/soft covering
Romito 8	Epigravettian[m] (ca. 14 ka cal. BP)	Italy	Hunter-gatherer	High	Unshod/soft covering
Romito 9	Epigravettian[m] (17−16 ka cal. BP)	Italy	Hunter-gatherer	High	Unshod/soft covering
Paglicci 164	Epigravettian[n] (19−13 ka)	Italy	Hunter-gatherer	High	Unshod/soft covering
Holocene hunter-gatherers (*n* = 15)					
Black Earth	Late Archaic[o] (~4950 cal BP)	Illinois, USA	Hunter-gatherer	High	Unshod/soft covering
Agriculturalist (*n* = 20)					
Norris Farms	Middle Woodland[p] (~650 cal BP)	Illinois, USA	Mixed agriculture and foraging	Intermediate	Unshod/soft covering
Post-industrial (*n* = 39)					
Bologna	19th−20th century[q]	Italy	Postindustrial	Low	Heavy shoes/boots

[a] The Clark Howell talus from Omo, Ethiopia, has not yet been dated but is constrained by deposits yielding other dated fossil specimens (Pearson et al., 2008; Parr et al., 2014).
[b] Rink et al. (1995).
[c] Grün and Stringer (2000).
[d] Pablos et al. (2019).
[e] Rink et al. (2001).
[f] Pomeroy et al. (2020).
[g] Guérin et al. (2015).
[h] Grün and Stringer (1991).
[i] Semal et al. (2009).
[j] Ronchitelli et al. (2015).
[k] The layer has been ^{14}C dated to 22,200 ± 360 and to 22,110 ± 330 BP (uncalibrated; Mallegni et al., 2000). The date was Cal BP by Oxcal v. 4.2.3 using the calibration curve IntCal13.
[l] Vercellotti et al. (2008).
[m] Craig et al. (2010).
[n] Paglicci 164 is from an ancient/evolved Epigravettian reworked area, its exact date is unknown (Condemi et al., 2014).
[o] Jefferies (2013).
[p] Santure et al. (1990).
[q] Belcastro et al. (2017).

neck, and a more medially oriented talar neck/head. These talar features are overall interpreted as broader ranges of talar motions and slightly divergent hallux in hunter-gatherers than in sedentary people with low levels of distance traveled (Turley et al., 2015; Sorrentino, 2020b). Some of these features have been also described for Middle/Early Late Pleistocene hominins, likely suggesting a relationship between talar morphology and unshod, intense, locomotor regimes (Pablos et al., 2015, 2017; Pearson et al., 2020). Thus, we expect Neanderthal external morphology to be more similar to that of *H. sapiens* engaged in a mixed foraging/hunter-gatherer lifestyle.

In addition to subsistence and mobility strategies, we also tested the effect of allometry and genetic background as they are expected to contribute to differences in bone morphologies (Turley et al., 2015; Rosas et al., 2017; Sorrentino et al., 2020b). In particular, the early anatomically modern human Clark Howell talus (Pearson et al., 2008; Parr et al., 2014) from Omo (Ethiopia) will be informative in identifying potential ancestral traits in Neanderthal tali because its shared characters with Neanderthals would be suggestive of inherited traits from a common ancestor. Alternatively, such shared characters, if reflecting plastic responses, could be indicative of greater levels of physical activity in Middle/Early Late Pleistocene hominins in contrast to decreased levels of biomechanical stress in modern humans (Trinkaus, 1983, 2006; Chirchir et al., 2015; Ryan and Shaw, 2015).

Internally, we hypothesize similar patterns of variation in BV/TV and DA between Neanderthals and *H. sapiens* groups as both are committed bipeds. However, as greater trabecular density and alignment have been linked to increased levels of mobility and physical activities in humans (Chirchir et al., 2015; Ryan and Shaw, 2015; Saers et al., 2018; Stephens et al., 2018; DeMars et al., 2020), we expect relatively higher BV/TV and DA in Neanderthals, presumably reflecting their highly repetitive loading associated with longer bipedal travel, even when compared with Holocene hunter-gatherers (Shaw and Stock, 2013).

We do not have an expectation as to whether external landmark coordinates and internal point clouds of site-specific trabecular variables will covary. To our knowledge, no previous study has directly examined covariation between talar external and internal morphology; thus, ours is an exploratory study.

2. Materials and methods

2.1. Population description

Tali from 10 Neanderthals (Krapina 235 and Krapina 237, La Chapelle-aux-Saints, La Ferrassie 1 and La Ferrassie 2, Tabun C1, Spy 2, Shanidar 5, Amud 1, and Regourdou 1) ranging chronologically from ~130 to 40 ka were compared with 81 tali of *H. sapiens* representing four groups (Upper Paleolithic hunter-gatherers, Holocene hunter-gatherers, agriculturalists, and postindustrial), categorized according to inferred mobility and subsistence from archaeological records (Table 1). Upper Paleolithic hunter-gatherers ($n = 7$) belong to Gravettian (Veneri 2 and Paglicci 25) and Epigravettian (Romito 7, Romito 8, Romito 9, Paglicci 164, and Villabruna) periods in Italy (Mallegni et al., 2000; di Cesnola, 2003; Giacobini, 2006; Vercellotti et al., 2008; Craig et al., 2010; Condemi et al., 2014; Ronchitelli et al., 2015). Tali from Holocene hunter-gatherers ($n = 15$) dating to the Late Archaic period (~4950 cal BP) are represented by individuals from the Black Earth site (Carrier Mills Archaeological District, Illinois, USA), who are thought to have included an intense locomotor component in their habitual ranging activities based on archaeological evidence of their hunting and foraging subsistence strategy (Jefferies, 2013; Saers et al., 2018; DeMars et al., 2020; Sorrentino et al., 2020). The intermediate

mixed agricultural and hunting group ($n = 20$) consists of individuals belonging to the Middle Woodland Oneota site (~650 cal BP) of Norris Farms #36 (Illinois, USA), who had a mixed economy based on agriculture, foraging, and hunting; thus, they are thought to have had an intermediate level of mobility (i.e., moderate distance traveled) between highly terrestrially mobile hunter-gatherers and sedentary people (Santure et al., 1990; Saers et al., 2018; DeMars et al., 2020; Sorrentino et al., 2020b). The sedentary group is composed of individuals ($n = 39$) belonging to the post−industrial revolution period (19th−20th century) in Bologna (Italy). They are part of the identified human skeletal collection of the Certosa cemetery, and archival data on occupation exist for a majority of adult individuals in this modern urban society (Belcastro et al., 2017).

Aside from the tali with clear cultural attributions, we also analyzed the early anatomically modern *H. sapiens* Clark Howell talus from Omo, Ethiopia (Parr et al., 2014). Although not directly dated, the talus was recovered from deposits that have yielded other fossil specimens dating from 104 ± 7 ka to 196 ± 2 ka (Pearson et al., 2008).

Subsistence for each group was characterized as hunting and gathering, mixed agriculture and foraging, or postindustrial economy (Sorrentino et al., 2020b; Table 1). Neanderthals are thought to have primarily relied on hunting and gathering (Pearson et al., 2006), similar to Middle Stone Age *H. sapiens* (Faith, 2008), Upper Paleolithic individuals from Italy (Mallegni et al., 2000; Vercellotti et al., 2008; Craig et al., 2010), and Holocene Black Earth individuals from the USA (Jefferies, 2013). While the Black Earth group occupied multiseason forager base camps and based their subsistence mainly on hunting medium-sized fauna (Lopinot and Lynch, 1979; Brietburg, 1980; Jefferies, 2013), the Norris Farms (USA) group was mainly involved in the production of domesticated beans, maize, and squash and also in foraging for nuts, fishing, and hunting deer and bison. Thus, the Norris Farms group is thought to have practiced a mixed economy based on both agriculture and foraging (Santure et al., 1990). Lastly, Bologna individuals (Italy) based their subsistence on different labors and specializations (agrarian, maritime, agricultural, and urban) in a postindustrial economy (Belcastro et al., 2017).

Inferring levels of mobility in past populations is difficult as it is based on archaeological records. Here, mobility refers to locomotion (e.g., distance traveled), and it was characterized as a gradation: high+ (extremely mobile), high (mobile), intermediate (i.e., semisedentary), and low (i.e., sedentary; Sorrentino et al., 2020b; Table 1). High + characterized Neanderthals and Gravettian individuals, following from literature suggesting mobility demands greater than those of hunter-gatherers from the Epigravettian and Holocene. This categorization follows from the interpretation of prehistoric hominin activity based on bone robusticity (e.g., cross-sectional geometry of the femur and relative tibial strength), estimated energetic costs of foraging (e.g., based on lower limb length and body mass), and technocomplex and climatic reconstructions that have led to a hypothesized decrease in mobility from the Late Upper Paleolithic, probably due to reduction of available territory and resources after the Last Glacial Maximum (Holt, 2003; Weaver and Steudel-Numbers, 2005; Holt and Formicola, 2008; Shaw and Stock, 2013). Within the Holocene period, the main difference lies in the adoption of sedentarism, which could be considered partial in the case of the mixed agriculture and foraging subsistence group (e.g., Norris Farms) and total in the case of the industrial group (e.g., Bologna sample).

Typical footwear was characterized as unshod/minimally shod and heavy leather shoes/boots, with the assumption being that prehistoric human groups belonged to the former category (Trinkaus, 2005; Sorrentino et al., 2020b). Even if there are few

examples, footprints of early anatomically modern humans in Africa and Neanderthals in Europe attest to the fact that they performed barefoot walking (Onac et al., 2005; Lockley et al., 2008). Trinkaus (2005) has suggested that the use of foot coverings became frequent by the Middle Upper Paleolithic, but footprints in European Upper Paleolithic caves attest to these populations frequently performing barefoot walking as well (Trinkaus, 2005; for a review, refer to the study by Lockley et al., 2008). The use of sandals is suggested in the North American Southwest around ca. 9000 BP (Geib, 2000), but this footwear was likely not hard soled and rigid similar to modern shoes (Willems et al., 2017, 2021).

2.2. Data collection

Three-dimensional (3D) surface reconstructions of 92 tali (82 *H. sapiens* and 10 Neanderthals) were acquired using either laser, computed tomography (CT), or microCT scans, which are known to give comparable results (Brzobohatá et al., 2012; Waltenberger et al., 2021). To estimate the impact of using meshes generated from different procedures on the present analyses, we performed a topological analysis of distances among vertices (using the 'meshdist' function of the R package 'Morpho' v. 2.8; Schlager, 2017) on 10 tali from the Bologna sample acquired both with CT and microCT systems. Comparisons between the CT- and microCT-generated meshes yielded an average deviation of 0.538 ± 0.254 mm (SOM Table S1), showing mostly smaller deviations on talar facet outlines and larger deviations corresponding to holes and areas where the trabecular bone is exposed (SOM Fig. S2). Overall, the average deviation does not show a high discrepancy between CT- and microCT-generated meshes, and it is well within the defined resolution (0.7 mm) of the CT scan-generated models.

Avizo v. 9.2 (Thermo Fisher Scientific, Waltham) was used to generate digital 3D models (isosurface reconstructions) from microCT/CT data. In most cases, left tali were used, but when unavailable (e.g., fossil remains), the right talar was mirrored for geometric morphometric analysis. Raw data from microCT/CT scans were reconstructed as 16-bit unsigned TIFF or DICOM images.

CT scans of Krapina 235 (voxel size: $0.154 \times 0.154 \times 0.400$ mm) and Krapina 237 (voxel size: $0.158 \times 0.158 \times 0.400$ mm) were obtained from Neanderthal Studies Professional Online Service (NESPOS; http://www.nespos.org). Those of La Chapelle (voxel size: $0.212 \times 0.212 \times 0.335$ mm), La Ferrassie 1 (voxel size: $0.219 \times 0.219 \times 0.400$ mm), and La Ferrassie 2 (voxel size: $0.251 \times 0.251 \times 0.500$ mm) were kindly provided by the Museum National d'Histoire Naturelle, Département Hommes, Natures, Sociétés (Paris, France).

Surfaces from Tabun C1, Spy 2, and the Clark Howell Omo talus (Omo deposits, Ethiopia) were taken from casts housed at the Natural History Museum of London (Palaeontology Department Collection) using a Konica Minolta Vivid 910 laser scanner (X: ± 0.22 mm, Y: ± 0.16 mm, Z: ± 0.10 mm) and reconstructed with the associated software (Polygon Editing Tool− PET 2006) in conjunction with Geomagic Studio v. 8 (3D System, Rock Hill).

The Shanidar 5 talus was microCT scanned at the Cambridge Biotomography Centre, University of Cambridge (Cambridge, UK), using a Nikon XTH 225 ST HRCT at a voxel resolution of 0.047 mm (125 kV, 135 μA).

The Amud 1 talus was microCT scanned at the Shamunis Family Anthropology Institute, Sackler Faculty of Medicine at the Tel Aviv University (Tel Aviv, Israel) using a Nikon XT H 225 ST at a voxel resolution of 0.030 mm (195 kV, 123 μA).

The talus of Regourdou 1 was microCT scanned at the European Synchrotron Radiation Facility (Grenoble, France), using a monochromatic X-ray beam, energy settings of 70 kV, high photon flux

$(2.10^{14}$ ph/s, 0.1% bw, 0.1 A), and voxel resolution of $0.0455 \times 0.0455 \times 0.0457$ mm.

Five Upper Paleolithic hunter-gatherer tali (Romito 7, Romito 8, Romito 9, Veneri 2, and Paglicci 164) were surface scanned using a 3D ARTEC scanner at the Department of Cultural Heritage, University of Bologna (Bologna, Italy). The tali of Paglicci 25 and Villabruna were microCT scanned at the Department of Physics and Astronomy, University of Bologna (Bologna, Italy), using an in-house CT system (Kevex PXS10-65 microfocus X-ray tube and Varian PaxScan 2520D flat-panel X-ray detector; Albertin et al., 2019) at an isotropic voxel resolution of 0.040 mm (78 kV, 200 μA).

Tali from Bologna were CT scanned using a 64-slice Brilliance Philips Medical System (Eindhoven, Netherlands), housed at the Department of Diagnostic Imaging of Santa Maria delle Croci Hospital (Ravenna, Italy) with a voxel resolution of $0.960 \times 0.960 \times 0.700$ mm at 140 kVp and an exposure time of 1645 ms.

A subsample of the Bologna tali ($n = 10$) was microCT scanned along with the Norris Farms and Black Earth tali using the OMNI-X HD600 high-resolution X-ray computed tomography (HRCT) system at the Center for Quantitative Imaging (CQI) at the Pennsylvania State University (University Park, Pennsylvania) with a voxel resolution between 0.030 and 0.057 mm (2800−4800 views, 180 kV, 110 μA).

2.3. Geometric morphometric analysis

Complete geometric morphometric talar morphology and individual talar articular facets were investigated using a 3D template of 251 (semi) landmarks (described in detail in the study by Sorrentino et al., 2020a, b, c), applied in Viewbox v. 4 (dHAL software, Kifissia). To obtain geometrically homologous semilandmarks, curve and surface semilandmarks were allowed to slide along the curves/surfaces to minimize thin-plate spline (TPS) bending energy between the target and template (Gunz and Mitteroecker, 2013). In cases where Neanderthal tali were damaged (SOM Table S2), a digital reconstruction was conducted based on a (semi)landmark estimation procedure (Gunz and Mitteroecker, 2013; Sorrentino et al., 2020a) referencing the Neanderthal mean shape derived from La Ferrassie 1 and 2, Spy 2, and Tabun C1.

The (semi)landmark coordinates were superimposed by generalized Procrustes analysis (GPA) using the package 'Geomorph' v. 3.3.1 (Adams and Collyer, 2020) for R v. 3.6.1 (R Core Team, 2019), with semilandmarks being allowed to slide with each recursive update of the Procrustes consensus (Slice, 2005). Separate GPAs were performed for raw coordinates of the complete talus and for each individual articular facet (Sorrentino et al., 2020a).

Principal component analysis (PCA) was performed on Procrustes coordinates, and shape changes along the principal axes were obtained by TPS deformation of the Procrustes mean shape surface (Bookstein, 1991) in Avizo v. 9.2. Shape differences between means of Neanderthal and *H. sapiens* groups were visualized as heatmaps using the 'meshdist' function of the R package 'Morpho' v. 2.8 (Schlager, 2017). Following TPS interpolation of the Procrustes mean shape with the mean (semi) landmark sets of each group (i.e., Neanderthal, Upper Paleolithic hunter-gatherer, Holocene hunter-gatherer, agriculturalist, and postindustrial groups), 'meshdist' calculates the distance between the vertices of a reference mesh (i.e., the Neanderthal mean) and target meshes (i.e., the Upper Paleolithic hunter-gatherer, Holocene hunter-gatherer, agriculturalist, and postindustrial means, respectively). Distance is then mapped to the reference mesh using color to visually indicate if the vertex of a target mesh falls within (blue) or outside (red).

Shape differences among groups were tested through Procrustes analysis of variance (ANOVA) using a residual randomization

procedure ($n = 1000$) and a pairwise function from the 'RRPP' package v. 0.5.2 (Collyer et al., 2015; Collyer and Adams, 2018) applying false discovery rate (FDR) correction of p-values obtained from pairwise Procrustes ANOVA (Benjamini and Hochberg, 1995; Theska et al., 2020).

Talus centroid size (i.e., square root of the summed squared distances between each semilandmark and the centroid of the semilandmark configuration) was used as a proxy for body mass and overall talar size (Parr et al., 2011). Differences in talar size were tested using a Kruskal−Wallis test followed by a Mann−Whitney U intergroup comparison and then visualized using boxplots. Talar shape variation ascribable to a logarithm of the centroid size across the sample (shape ~ logarithm of the centroid size) was assessed through a Procrustes ANOVA.

A Procrustes ANOVA was performed to assess if group shape differences were a manifestation of shape allometry (shape ~ groups × logarithm of the centroid size) or are influenced by subsistence strategy, mobility, or footwear, respectively (Table 2). There may very well be interactions between some of these variables, but the small sample size of the present study does not allow this to be assessed statistically.

Finally, pairwise comparisons ('RRPP' package) based on Procrustes ANOVAs were performed to calculate distances between categories across permutations for each variable (i.e., subsistence strategy, mobility, and footwear) using an FDR correction of p-values following Theska et al. (2020).

In sum, a total of six Procrustes ANOVAs (i.e., group, size, group:size, subsistence, mobility, and footwear) were performed for each of the Procrustes coordinates data sets (i.e., whole talus and individual facets, separately) and FDR correction of p-values (Benjamini and Hochberg, 1995) was used as a multiple testing correction.

Table 2
Procrustes analyses of variance (ANOVA) for whole talus and individual facets.[a]

Variables	Df	SS	MS	R^2	F	Z	p-value	p-adj.
Whole talus								
Group	4	0.12940	0.03235	0.20189	5.5178	10.2352	**0.001**	**0.001**
Size	1	0.01042	0.01042	0.01626	1.7772	2.5982	**0.005**	**0.007**
Group:size	4	0.02623	0.00655	0.04093	1.1186	1.4082	0.075	0.082
Subsistence	2	0.08469	0.04234	0.13214	7.1192	8.4757	**0.001**	**0.001**
Mobility	3	0.11196	0.03732	0.17469	6.1382	9.3445	**0.001**	**0.001**
Footwear	1	0.07070	0.07070	0.11031	11.0350	7.8307	**0.001**	**0.001**
Posterior calcaneal facet								
Group	4	0.11864	0.02966	0.14289	3.7480	5.4593	**0.001**	**0.001**
Size	1	0.03028	0.03028	0.03647	3.8268	3.3410	**0.001**	**0.001**
Group:size	4	0.04035	0.01008	0.04860	1.2747	1.4453	0.074	0.082
Subsistence	2	0.05545	0.02772	0.06678	3.1486	3.8682	**0.001**	**0.001**
Mobility	3	0.09693	0.03231	0.11674	3.8329	5.0685	**0.001**	**0.001**
Footwear	1	0.03358	0.03358	0.04045	3.7516	3.2005	**0.001**	**0.001**
Trochlea								
Group	4	0.12576	0.03143	0.18348	4.8946	6.6970	**0.001**	**0.001**
Size	1	0.00511	0.00511	0.00746	0.7956	−0.2711	0.597	0.611
Group:size	4	0.03425	0.00856	0.04997	1.3330	1.6531	**0.048**	0.057
Subsistence	2	0.07214	0.03606	0.10525	5.1755	5.2898	**0.001**	**0.001**
Mobility	3	0.09584	0.03194	0.13982	4.7140	5.7289	**0.001**	**0.001**
Footwear	1	0.05624	0.05624	0.08205	7.9556	4.8771	**0.001**	**0.001**
Navicular facet								
Group	4	0.15477	0.03869	0.17202	4.4896	5.6037	**0.001**	**0.001**
Size	1	0.01981	0.01981	0.02202	2.2986	2.1146	**0.016**	**0.021**
Group:size	4	0.02705	0.00676	0.03007	0.7848	−0.6544	0.738	0.738
Subsistence	2	0.08293	0.04146	0.09217	4.4673	4.4590	**0.001**	**0.001**
Mobility	3	0.11196	0.03732	0.17469	6.1382	9.8315	**0.001**	**0.001**
Footwear	1	0.06202	0.06201	0.06893	6.5889	4.0457	**0.001**	**0.001**
Lateral malleolar facet								
Group	4	0.20717	0.05179	0.21970	6.1731	5.8798	**0.001**	**0.001**
Size	1	0.02606	0.02605	0.02763	3.1057	2.5630	**0.009**	**0.012**
Group:size	4	0.03017	0.00754	0.03199	0.8989	−0.0395	0.521	0.547
Subsistence	2	0.15003	0.07501	0.15910	8.3248	5.5507	**0.001**	**0.001**
Mobility	3	0.19688	0.06562	0.20879	7.6528	5.6717	**0.001**	**0.001**
Footwear	1	0.11965	0.11965	0.12689	12.9340	4.8786	**0.001**	**0.001**
Medial malleolar facet								
Group	4	0.15960	0.03990	0.18667	5.1118	5.3355	**0.001**	**0.001**
Size	1	0.01736	0.01735	0.02030	2.2236	1.7219	**0.048**	0.057
Group:size	4	0.04580	0.01145	0.05357	1.4669	1.4390	0.073	0.082
Subsistence	2	0.10201	0.05100	0.11930	5.9604	4.8822	**0.001**	**0.001**
Mobility	3	0.12165	0.04054	0.14227	4.8103	4.8538	**0.001**	**0.001**
Footwear	1	0.08498	0.08498	0.09939	9.8224	4.4339	**0.001**	**0.001**
Anterior-medial calcaneal facet								
Group	4	0.40889	0.10222	0.23600	6.8262	6.4382	**0.001**	**0.001**
Size	1	0.03692	0.03691	0.02131	2.4652	1.9571	**0.025**	**0.031**
Group:size	4	0.07382	0.01845	0.04261	1.2324	0.8763	0.202	0.217
Subsistence	2	0.17871	0.08935	0.10314	5.0603	4.1219	**0.001**	**0.001**
Mobility	3	0.37521	0.12506	0.21656	8.0161	5.6576	**0.001**	**0.001**
Footwear	1	0.10825	0.10825	0.06248	5.9313	3.2929	**0.001**	**0.001**

Abbreviations: Df = degree of freedom; SS = Procrustes distance sum of squares; MS = mean squares distance; R^2 = coefficient of determination; F = effect type; Z = effect size.
[a] Shape differences were evaluated for model terms: group, size (logarithm of centroid size), allometric effect (group:size), subsistence, mobility, and footwear. Significant p-values (<0.05) for model terms and false discovery rate (FDR) correction of p-value (p-adj.) are in bold.

2.4. Image segmentation and trabecular analysis

Trabecular analysis was conducted on a subsample of individuals with available microCT scans. These included Neanderthals (Regourdou, Shanidar, Amud), Upper Paleolithic hunter-gatherers (Paglicci 25 and Villabruna), Holocene hunter-gatherers ($n = 13$), agriculturalists ($n = 17$), and a subsample of postindustrial ($n = 10$) individuals (Gross et al., 2014). TIFF/DICOM stacks of images were recast as TIFF unsigned 8-bit in ImageJ v. 1.52a (Schneider et al., 2012) and segmented using the K-means with fuzzy C-means clustering algorithm described in the study by Dunmore et al. (2018). When necessary (e.g., excessive sediment/bright inclusions), tali were manually prepared in Avizo v. 9.2, using the paintbrush tool (e.g., removing sediment and matrix) before segmentation.

Quantification of BV/TV and DA was performed by isolating trabecular from cortical bone in Medtool v. 4.3 (Gross et al., 2014). Values reported here represent the mean from a series of 7.5 mm volumes of interest (VOI) taken at each 3.5-mm-spaced node of a grid overlapping the talar volume. Results for BV/TV and DA are visualized on a tetrahedral mesh by interpolating the results for these VOIs into the centroid of each tetrahedron (Gross et al., 2014).

To statistically compare different groups, we followed the protocol proposed by DeMars et al. (2020), where point clouds were used to create site-specific means for each group, following a 3D implementation of the workflow described in the study by Stephens et al. (2018). In brief, each individual mesh was globally aligned using pseudolandmarks automatically positioned by a modified version of the 'auto3dgm' in 'Geomorph' v. 3.3.1, R package (Boyer et al., 2015; Tingran et al., 2020) and a GPA was performed to find the mean shape coordinates. The mesh representing the individual closest to the mean was deformed along the mean shape coordinates using 'Geomorph' v. 3.3.1 (Adams and Collyer, 2020). A point cloud of the mean (canonical) mesh was then registered rigidly, affinely, and deformably to each of the individual point clouds in Python v. 3.7 (Python Software Foundation, Wilmington), and the associated values were then linearly interpolated to the canonical point using the phenotypic cloud analysis package (DeMars et al., 2020; Stephens, 2020). To identify significant differences in site-specific BV/TV and DA, a two-tailed *t*-test was performed between homologous values within the point cloud of two groups. *P*-values for multiple tests were corrected using random field theory following Worsley et al. (1996), and the resulting *t*-scores were mapped on the canonical point cloud (DeMars et al., 2020). Following these steps, the mean point cloud was then reassociated with the mean mesh and the group averages, their respective coefficients of variation, and the *t*-scores for the pairwise statistical results were visualized in Paraview v. 5.7.0 (Ayachit, 2015).

2.5. Covariation between talar shape and trabecular structures

Both external and internal bone morphology respond to functional loading, with changes in external bone shape, size, and orientation of articular surfaces facilitating joint motions during habitual locomotor behaviors, while trabeculae increase in density and spatial organization to better transfer biomechanical loads internally, away from joint surfaces. Even so, external bone morphology is thought to be under tighter genetic control, especially the articular areas, to maintain joint congruence between articulating tarsal bones. In contrast, trabecular bone may model its architecture within the bone throughout an organism's life, with the density and primary orientation being maintained in adulthood through repeated loading (Lieberman et al., 2001; Ruff et al., 2012; Kivell, 2016).

Therefore, we test potential covariation between external talar morphology and trabecular structure variation to understand if both reflect adaptation to the same biomechanical forces (e.g., forces feet may experience while walking unshod long distances versus feet of individuals with a sedentary lifestyle and wearing rigid-soled shoes).

An extended geometric morphometric analysis was used to estimate the relationship between biomechanical properties and morphology of the talus of matching individuals. A partial least squares (PLS) regression was used to measure the degree of covariation between Procrustes shape coordinates and the pseudolandmark values of BV/TV and DA, respectively. These relationships were assessed using the two-block function provided in the R package 'Geomorph' v. 3.3.1 (Adams and Collyer, 2020), whereby random permutations of the individuals ($n = 1000$) are used to build a distribution of values. The null hypothesis is that the variables are independent, with covariation being measured by the r coefficient and statistical significance ($p < 0.05$) being achieved when the blocks are correlated (Rohlf and Corti, 2000). As sample size and the number of variables may affect the final results, multivariate effect size was considered to interpret the strength of the covariation signal across the sample (Adams and Collyer, 2016, 2019).

3. Results

3.1. Talar external morphology

A Procrustes ANOVA indicates that the main predictor for talar shape variation is group membership for the whole talus and the individual talar facets (Table 2). Whole talar shape is also strongly influenced by mobility followed by subsistence and footwear. Mobility also plays a role in influencing the shape of individual facets, while the other factors differentially contribute based on the facet considered (Tables 2 and 3, SOM Tables S3 and S4). For centroid size (i.e., size proxy), the whole talus and individual talar facets—except the posterior calcaneal and lateral malleolar facets—vary among groups (Figs. 1a, 2a, 3a, 4a, SOM Figs. S3a, S4a and S5a, and SOM Table S5). Centroid size explains (except for the trochlea and medial malleolar facet) from ~2 to 5% (see R^2) of shape variation across the individuals within the sample, but size does not account for allometric shape differences among groups (Table 2).

The Procrustes ANOVA (Tables 2 and 3) and PCA (Fig. 1b–d) for whole talar morphology differentiate Neanderthals from each *H. sapiens* group mostly along PC2 and PC3, as well as *H. sapiens* groups from one another (particularly the postindustrial group from the others along PC1). The Clark Howell talus falls closest to the Neanderthal convex hull in the PCA. Overall, complete talar configuration for the Neanderthal group differs from that of *H. sapiens* in being shorter, with an absolutely—and relative to the corpus—shorter neck and a broader head (see extreme shape along negative scores of PC2 and PC3 in Fig. 1c, d, and the red color of the talar head in Fig. 5 indicating that the *H. sapiens* head extends beyond the Neanderthal head because of the longer neck length of the former), which is the pattern observed in the Clark Howell talus as well (SOM Fig. S6). Medial and lateral tubercles are less inferiorly extended in the Neanderthal group, and the trochlea is more rectangular-shaped relative to talar proportions (extreme shape along negative scores of PC2 and PC3 in Fig. 1c, d; note the trend of the lateral side of the trochlea to become red from both *H. sapiens* hunter-gatherer to postindustrial groups in Fig. 5), which is a pattern observed in the Clark Howell talus and the Upper Paleolithic hunter-gatherers (SOM Fig. S6).

Pairwise Procrustes ANOVAs of individual articular facets show how Neanderthals differ from each *H. sapiens* groups (Table 3), with variation in the discriminatory power of individual facets (Table 2).

Table 3
Pairwise comparisons of Procrustes analyses of variance (ANOVA) results for the whole talus and individual articular facets.[a]

Talar region/surface	Neanderthal vs. Upper Paleolithic hunter-gatherer	Neanderthal vs. Holocene hunter-gatherer	Neanderthal vs. agriculturalist	Neanderthal vs. postindustrial	Upper Paleolithic hunter-gatherer vs. Holocene hunter-gatherer	Upper Paleolithic hunter-gatherer vs. agriculturalist	Upper Paleolithic hunter-gatherer vs. postindustrial	Holocene hunter-gatherer vs. agriculturalist	Holocene hunter-gatherer vs. postindustrial	Agriculturalist vs. postindustrial
Whole talus	**0.001**	**0.001**	**0.001**	**0.001**	**0.008**	**0.003**	**0.001**	0.142	**0.001**	**0.001**
Posterior calcaneal facet	**0.016**	**0.004**	**0.004**	**0.004**	0.053	**0.032**	0.097	0.548	**0.015**	**0.016**
Trochlea	**0.004**	**0.002**	**0.002**	**0.002**	**0.003**	**0.002**	**0.029**	0.556	**0.003**	**0.002**
Navicular facet	**0.022**	**0.002**	**0.002**	**0.002**	0.363	0.977	0.092	0.363	**0.002**	**0.002**
Lateral malleolar facet	**0.023**	**0.007**	**0.007**	**0.006**	0.487	0.062	**0.014**	0.060	**0.007**	**0.006**
Medial malleolar facet	**0.006**	**0.026**	**0.010**	**0.004**	**0.026**	**0.026**	0.065	0.692	**0.004**	**0.004**
Anterior-medial calcaneal facet	**0.002**	**0.002**	**0.002**	**0.002**	0.955	0.436	0.605	0.196	**0.020**	**0.002**

[a] Significant *p*-values (<0.05; with false discovery rate correction) for model terms are in bold.

In particular, morphology of the posterior calcaneal, anterior-medial calcaneal and navicular facets (Figs. 2−4) clearly distinguish Neanderthals from *H. sapiens* groups, more than that of the trochlea, medial and lateral malleolar facets (SOM Figs. S3−S5).

While the posterior calcaneal facet shows greater overlap among *H. sapiens* groups (Fig. 2b−d), Neanderthals separate from *H. sapiens* groups along PC2. By comparison, while Neanderthals again separate from *H. sapiens* groups in the anterior-medial calcaneal facet along PC1, this facet also tends to separate the postindustrial group from other *H. sapiens* groups mostly on PC3 (Fig. 3b−d). Relative to the *H. sapiens* groups, in Neanderthals the posterior calcaneal facet is enlarged (blue area in the distal calcaneal borders, Fig. 5) and flattened (red area indicating greater concavity in *H. sapiens* groups, Fig. 5) in its anterolateral aspect and slightly less concave (extreme shape on PC2 negative in Fig. 2c; see also SOM Fig. S6), with the anterior and middle calcaneal facets joining to form a slightly more convex and less posteriorly expanded facet (extreme shape on PC1 positive in Fig. 3d; see also SOM Fig. S6).

The PCA plot of the navicular facet (Fig. 4b−d) shows the Clark Howell talus within the Neanderthal convex hull, which itself overlaps slightly with that of Holocene hunter-gatherers. However, the Neanderthal and Clark Howell navicular facets differ from those of Upper Paleolithic and Holocene hunter-gatherers in having a mediolaterally broader (lateral and medial margin colored in blue, Fig. 5) and dorsoplantarly narrower navicular facet and a medial border of the talar head that extends posteriorly (extreme shape on PC1 positive in Fig. 4d; see also SOM Fig. S6).

PCA plots of the medial (SOM Fig. S3b−d) and lateral malleolar facets (SOM Fig. S4b−d) show great variability in the postindustrial group, and most of these individuals overlap with other *H. sapiens* groups. Neanderthals tend to plot in the same regions covered mostly by more mobile groups and, ultimately, those resembling them morphologically. While not as dramatic as differences in other facets, the Neanderthal lateral malleolar facets slightly differ from more mobile groups in presenting a relatively more flared lateral and more cupped medial malleolar facet (reddish regions in Fig. 5 indicating a more flattened surface in *H. sapiens* groups; SOM Figs. S3, S4 and S6).

The PCA plot for the trochlear facet (SOM Fig. S5b−d) shows great overlap among groups. The Neanderthal trochlear facet slightly differs morphologically in being relatively more dorsally convex than all other groups and with a slightly less deep central groove with respect to *H. sapiens* groups (blue area in the mid-anterior trochlear region, Fig. 5), but the anterior extension of the medial margin is similar to that observed in the more mobile groups (extreme shapes along PC1 positive, Fig. 1d).

3.2. Talar trabecular structure

Mean site-specific trabecular maps show generally similar distributions for BV/TV and DA throughout the talus among groups (Figs. 6 and 7). The highest BV/TV is found along the lateral aspect, anterior trochlear region, lateral and medial malleolar facets, the dorsolateral region of the head, and the posterior calcaneal facet (Fig. 6b). High DA is present along the dorsal aspect of the head and plantar to the central-lateral trochlear region (Fig. 7b).

For BV/TV, the coefficient of variation indicates that the Upper Paleolithic group has the most variable distribution with the postindustrial group being the most consistent (Fig. 6a, c). However, higher variability in BV/TV for Upper Paleolithic hunter-gatherers may be due, in part, to the small sample size. Overall, BV/TV is highest in the Neanderthal group and then the Upper Paleolithic group (Fig. 6b, c).
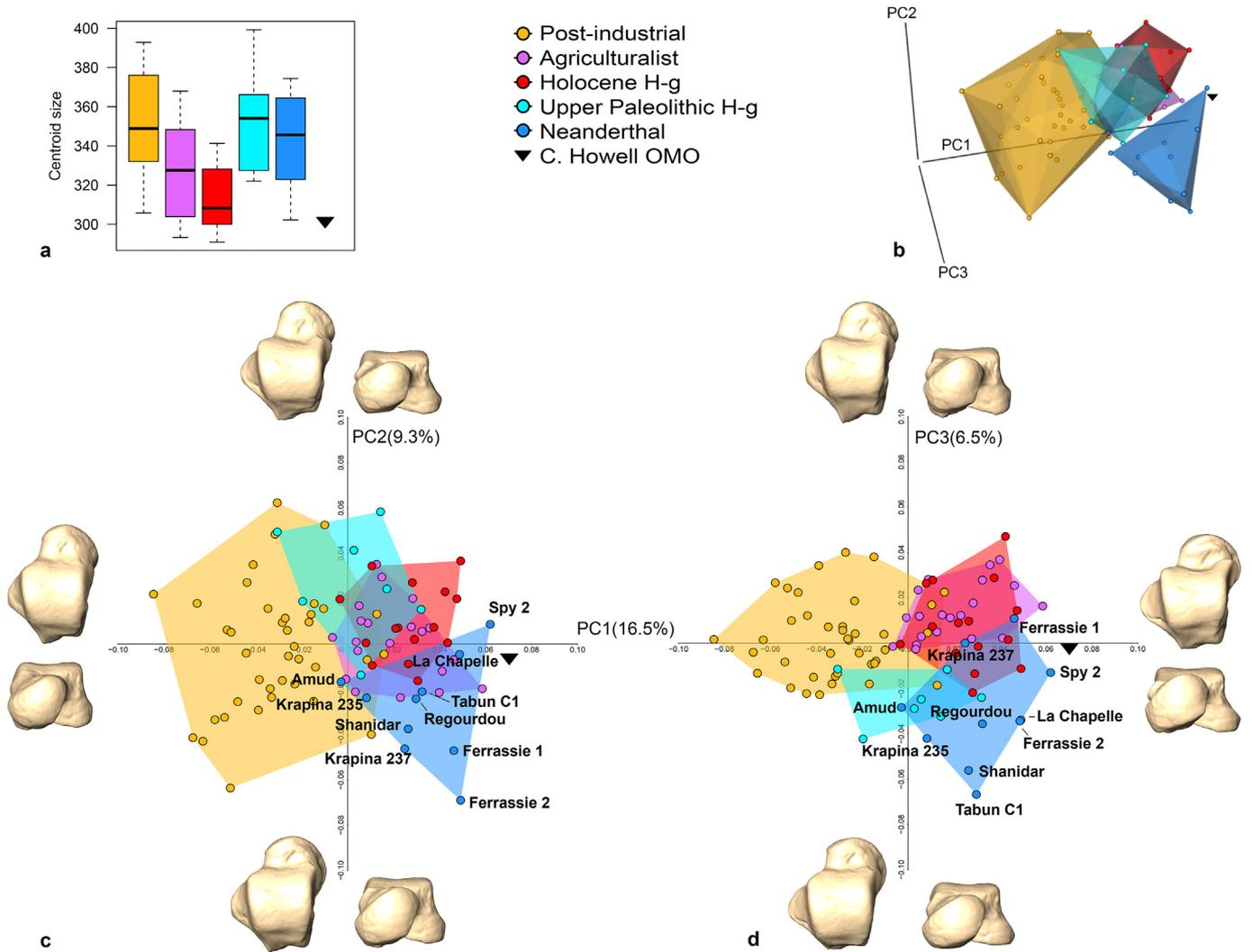
Figure 1. Principal component analysis (PCA) plots of the whole talus. A boxplot of the centroid size distribution by group is on the top left (a), where the horizontal bar indicates the median, the limits of boxes show upper and lower quartiles, and the terminus of whiskers shows extremes of each range. PC1−3 are shown in 3D on the top right (b), PC1 vs. PC2 on the bottom left (c), and PC1 vs. PC3 on the bottom right (d). Shape differences along the first three PCs are illustrated in dorsal and distal views (c, d). Abbreviation: H-g = hunter-gatherers. Please refer to the interactive 3D plot in SOM Fig. S7 for further details.

BV/TV site-specific pairwise comparisons indicate that the Neanderthal group differs in having significantly higher values than *H. sapiens* groups (Fig. 6d), with higher bone volume fraction being present in all sites of the talus. Among *H. sapiens* groups, the greatest differences are between the Holocene hunter-gatherer and agriculturalist groups, with negligible differences between Upper Paleolithic and Holocene hunter-gatherers. Note that, owing to the small sample size for Neanderthal and Upper Paleolithic groups, similar tests between these two groups were not performed and comparisons with other groups should be interpreted with extreme caution for both BV/TV and DA results.

For DA, the coefficient of variation indicates the Neanderthal and Upper Paleolithic groups are the most variable, in part likely caused by the small sample size, while the agriculturalist group is most consistent (Fig. 7a, c). More overlap between groups occurs for DA than for BV/TV, but site-specific values are generally higher in the Neanderthal group, followed by the Upper Paleolithic and Holocene hunter-gatherer groups (Fig. 7b, c).

DA site-specific pairwise comparisons indicate that the Neanderthal group has significantly higher DA throughout the neck than Holocene hunter-gatherers, but is lower than the agriculturalist group along the navicular facet and superior aspect of the trochlea (Fig. 7d). Among *H. sapiens* groups, significant differences between the Upper Paleolithic and Holocene hunter-gatherer groups are negligible, with the Holocene hunter-gatherer group having significantly lower values compared to remaining groups. The agriculturalist group has significantly higher DA on the superior aspect than the postindustrial group.

A PLS regression between talar shape and site-specific point cloud values for BV/TV (r = 0.692, *p* = 0.144, effect size = 1.088) and DA (r = 0.703, *p* = 0.114, effect size = 1.206) shows no significant covariation. Despite this, more mobile groups (e.g., Neanderthals and both Upper Paleolithic and Holocene hunter-gatherers) tend to cluster and are associated with high BV/TV and DA values, as well as a broad talar head, a short neck, and a more flared lateral malleolar facet (Fig. 8).

4. Discussion

Neanderthal and *H. sapiens* external talar morphologies matched our predictions, with the contribution of levels of mobility, subsistence, cultural innovation, and phylogenesis
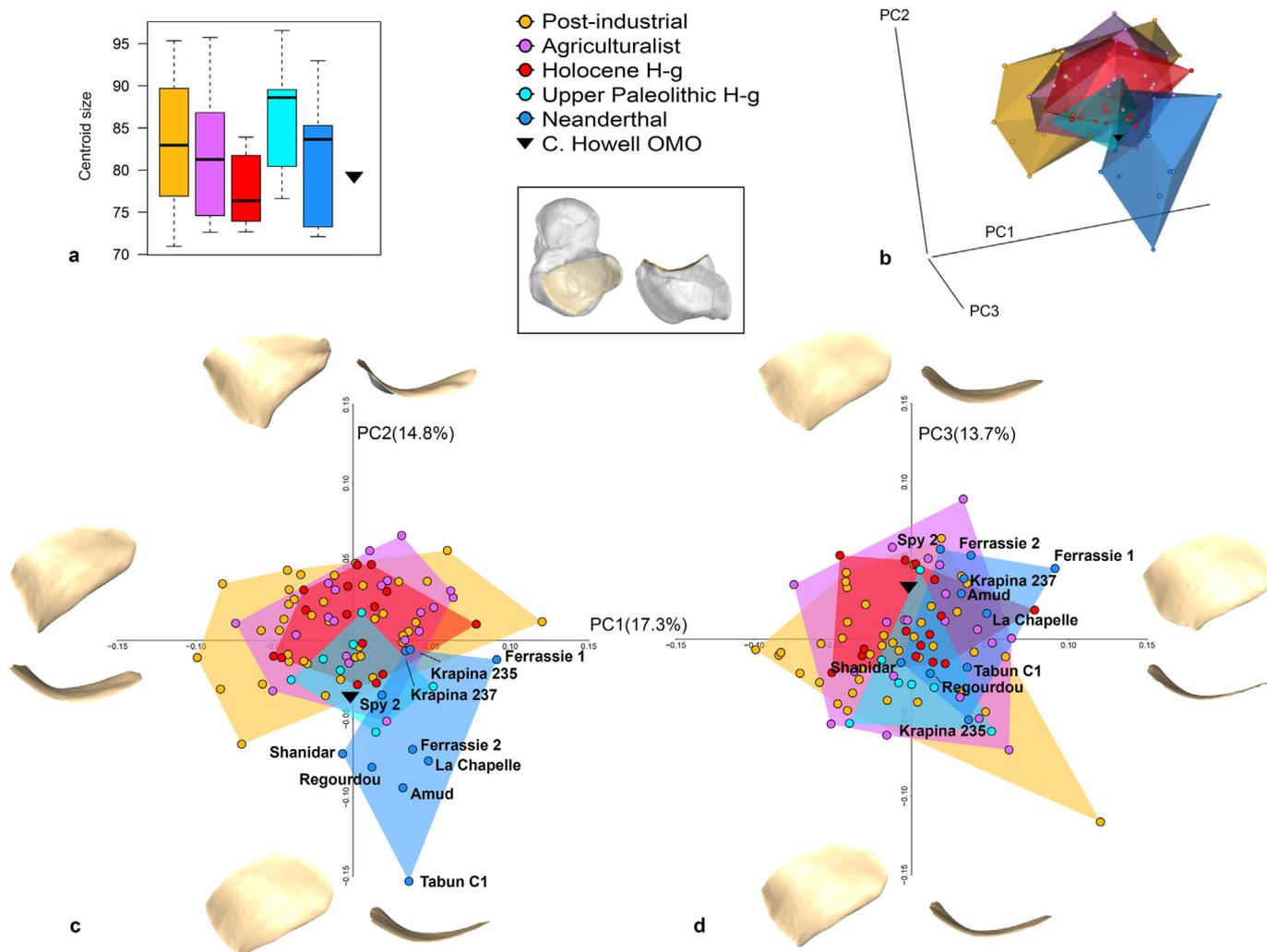
Figure 2. Principal component analysis (PCA) plots of the posterior calcaneal facet. A boxplot of the centroid size distribution by group is on the top left (a), where the horizontal bar indicates the median, limits of the boxes show upper and lower quartiles, and the terminus of whiskers shows extremes of each range. PC1−3 are shown in 3D on the top right (b), PC1 vs. PC2 on the bottom left (c), and PC1 vs. PC3 on the bottom right (d). Shape changes along the first three shape PCs are illustrated in plantar (top and left) and posterior lateral (bottom and right) views (c, d). Abbreviation: H-g = hunter-gatherers. Please refer to the interactive 3D plot in SOM Fig. S8 for further details.

resulting in distinct shape variations (Table 2). The prediction of greater talar robusticity and highly organized trabecular bone in more mobile Pleistocene and recent hunter-gatherers was also supported in the relatively high BV/TV and DA values observed in these groups (Figs. 6 and 7). Although Neanderthal talar external morphology and trabecular structure were distinct, external shape did not significantly covary with either BV/TV or DA (Fig. 8). This suggests that, at least for the talus, there is limited covariation between external and internal structures, which is in line with a view that external bone morphology (i.e., form of articular facets) is more developmentally canalized than trabecular structure and organization (Lieberman et al., 2001; Kivell, 2016). Additionally, it could be that external features (e.g., form of articular facets) are responsible for the range of motion in joints, while the trabecular bone underlying them is responsible for achieving bone (structural) integrity when they are under weight-bearing loads. Finally, characteristics exclusively shared between the anatomically modern Clark Howell talus and Neanderthals are likely to be ancestral traits or markers of robusticity reflecting Middle/Early Late Pleistocene activity patterns. These include being overall shorter, with less inferiorly and posteriorly projecting medial and lateral tubercles, a rectangular trochlea, a dorsoplantarly narrow navicular facet,

and—relative to the corpus—a shorter and broader neck and head (Figs. 1, 4, 5, and 9, SOM Fig. S6).

In regards to these potential ancestral traits, the Neanderthal and Upper Paleolithic groups have a trochlea similar to the Clark Howell talus in being relatively more rectangular relative to talar proportions (Figs. 1 and 5, SOM Fig. S6), which is a common morphology in Middle Pleistocene hominins (Pablos et al., 2017) suggesting that this configuration is ancestral for phylogenetic relationships. The Neanderthal talar neck is particularly short in relation to its elongated body, which is a common feature of Pleistocene *Homo* fossils, likely also indicative of an ancestral retention (Pablos, 2015).

Besides phylogenetic explanations, body mass has been indicated as a factor explaining the short and broad talar neck and head in Neanderthals. Previously, Rhoads and Trinkaus (1977) suggested an inverse relationship between talar neck length and trochlea length that reflects increased Neanderthal body mass, but more recent analyses suggest that the neck length is independent of talar body length (Rosas et al., 2017). Whatever the case, our results show that Neanderthal BV/TV in the neck is relatively high (Fig. 6), but it does not significantly differ from Holocene hunter-gatherers, where talar size (Fig. 1a, SOM Table S5) and body mass are also
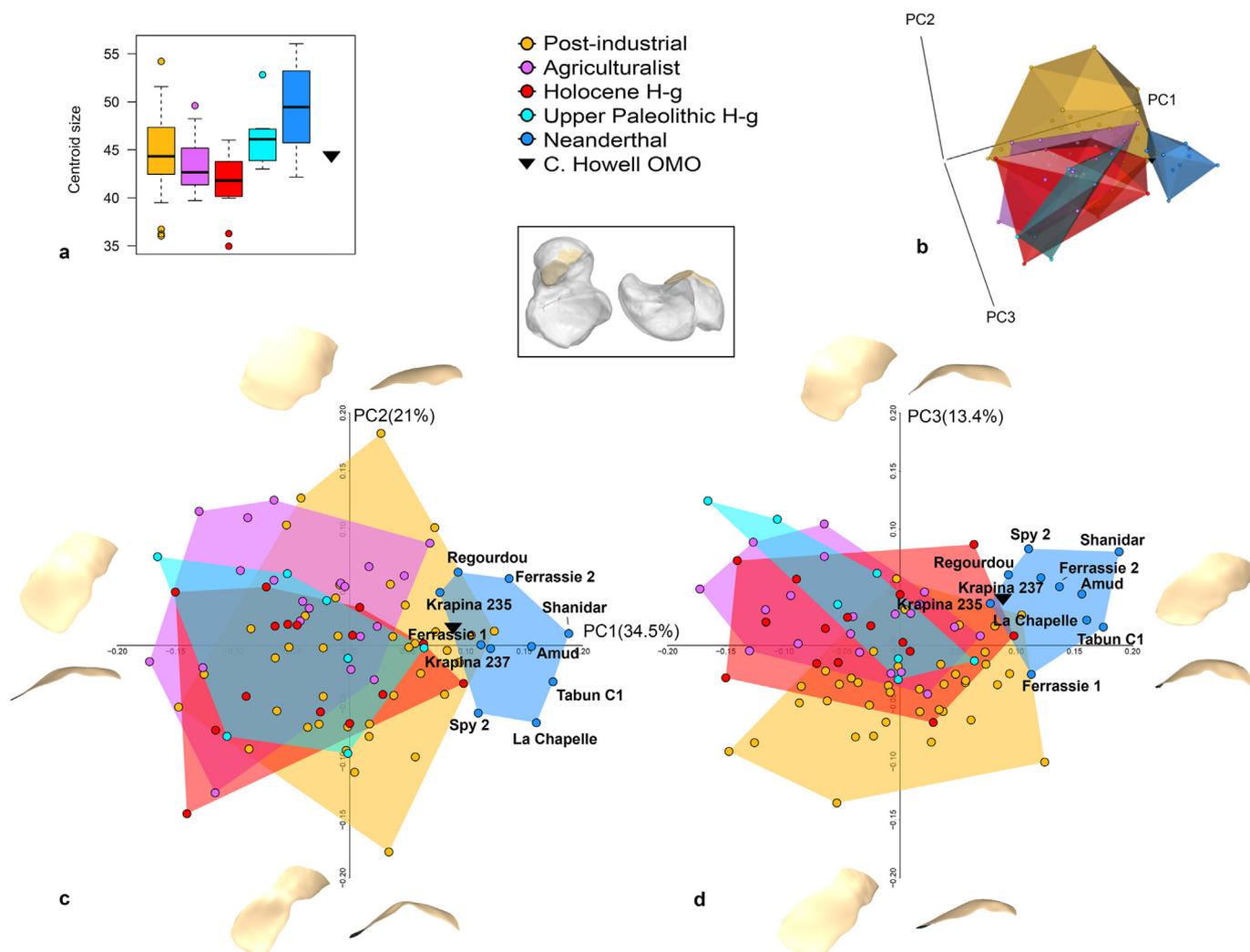
Figure 3. Principal component analysis (PCA) plots of the anterior-medial calcaneal facet. A boxplot of the centroid size distribution by group is on the top left (a), where the horizontal bar indicates the median, limits of the boxes show upper and lower quartiles, the terminus of whiskers shows the extremes of each range, and small circles are outliers. PC1—3 are shown in 3D on the top right (b), PC1 vs. PC2 on the bottom left (c), and PC1 vs. PC3 on the bottom right (d). Shape changes along the first three shape PCs are illustrated in plantar (top and left) and posterior lateral (bottom and right) views (c, d). Abbreviation: H-g = hunter-gatherers. Please refer to the interactive 3D plot in SOM Fig. S9 for further details.

reduced (cf. the femur head diameter in the studies by Plavcan et al., 2014 and Saers et al., 2019). Interestingly, DA was significantly different in the talar neck for these two groups, with values being higher in Neanderthals (Fig. 7). This suggests a higher amount of preferentially oriented trabecular struts in Neanderthals that may indicate a greater need to consistently transmit oriented loads, similar to those experienced by *H. sapiens groups* (except for Holocene hunter-gatherers). The talar neck of the Holocene hunter-gatherer group has extremely low DA and a low coefficient of variation that may indicate a common need to sustain more variably oriented loads (Fig. 7). Therefore, our results suggest that the external morphology of the talar neck is not related to body mass, but instead phylogenesis may better explain the short and broad neck of Neanderthals, whereas, internally, high BV/TV and DA suggest intense and oriented loading through the Neanderthal talar neck (Fig. 9).

Similarly, the broader talar head in Neanderthals and both Upper Paleolithic and Holocene hunter-gatherers is not related to allometric effects (Fig. 1 and Table 2). Rosas et al. (2017) found no correlation between the great extension of the talar head (navicular and calcaneo-navicular ligament facets) and body size, suggesting

that this may instead signal an anatomical and/or functional specialization in Neanderthals. Our results partially agree with those of Rosas et al. (2017), as we found significantly higher BV/TV in the Neanderthal talar head that is suggestive of intense levels of loading, likely from extreme mobility demands (Holt, 2003; Weaver and Steudel-Numbers, 2005; Pearson et al., 2006; Holt and Formicola, 2008; Shaw and Stock, 2013; Fig. 6). However, when compared with *H. sapiens* groups, we found that Neanderthal and Clark Howell tali possess an absolutely and relatively broader head than talar size (Pablos et al., 2019), with a dorsoplantarly narrow navicular facet (Figs. 1 and 5, SOM Fig. S6). This may indicate that the shape of the navicular facet, as well its relative proportions, is an ancestral condition or, at the very least, an indication of functional demands present in Middle Pleistocene hominins (Fig. 9). Indeed, the dorsoplantarly narrow navicular facet of hominins from Jinniushan suggests that they exhibited limited dorsal extension (Lu et al., 2011). Similarly, the mediolateral enlargement of the Neanderthal talar head is evident in some Middle Pleistocene hominins (Omo I, Jinniushan; Pearson et al., 2008; Lu et al., 2011), but not in remains from Sima de los Huesos (Pablos et al., 2017), which may indicate a demand for increased weight transfer along
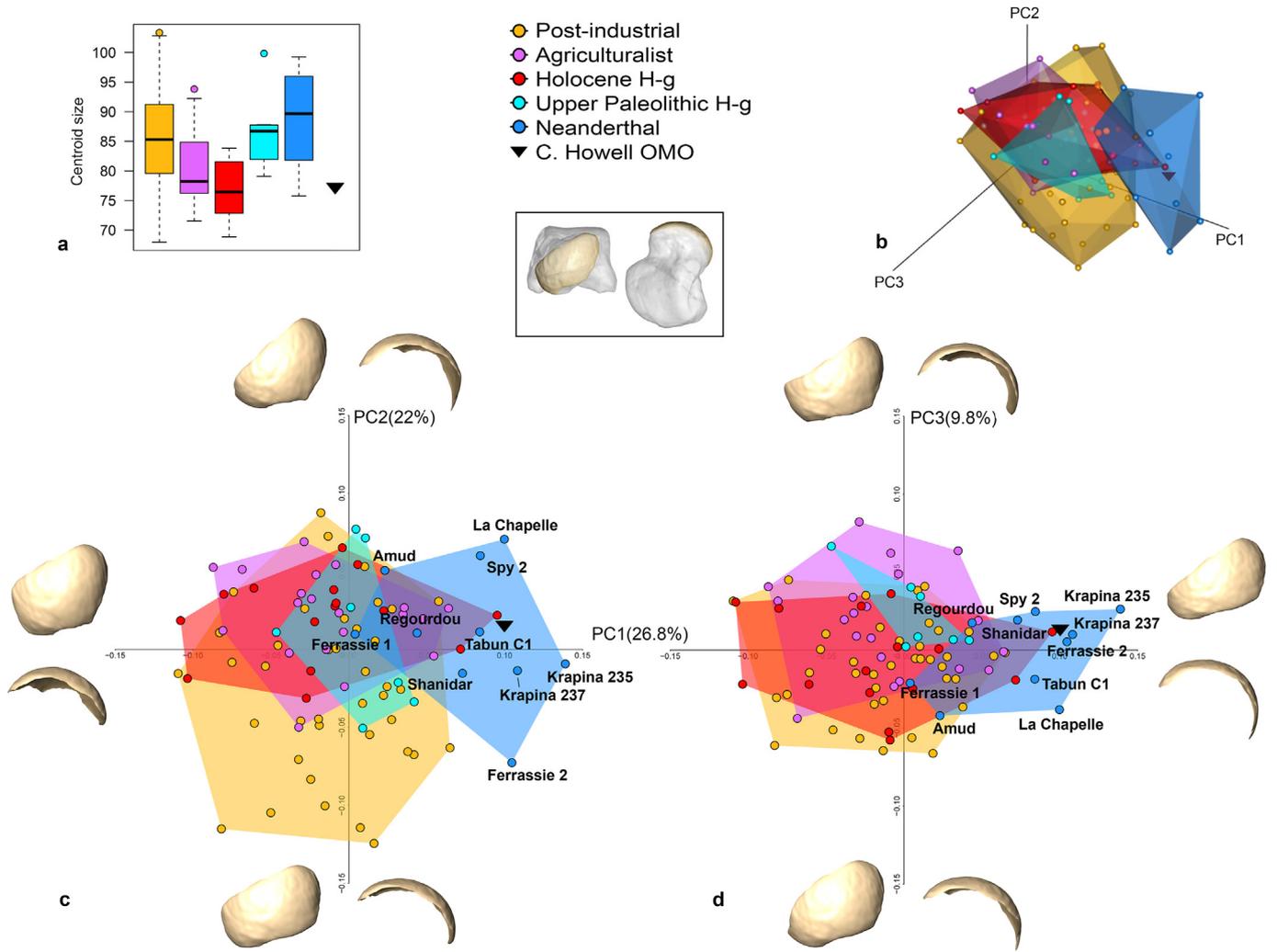
Figure 4. Principal component analysis (PCA) plots of the navicular facet. A boxplot of the centroid size distribution by group is on the top left (a), where the horizontal bar indicates the median, limits of the boxes show upper and lower quartiles, the terminus of whiskers shows extremes of each range, and small circles are outliers. PC1–3 are shown in 3D on the top right (b), PC1 vs. PC2 on the bottom left (c), and PC1 vs. PC3 on the bottom right (d). Shape changes along the first three shape PCs are illustrated in distal (top and left) and dorsal medial (bottom and right) views (c, d). Abbreviation: H-g = hunter-gatherers. Please refer to the interactive 3D plot in SOM Fig. S10 for further details.
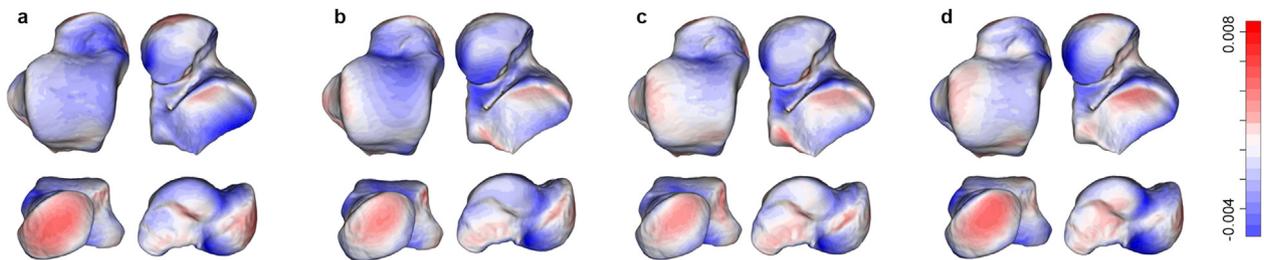
Figure 5. Displacement heatmaps showing talar shape differences between the Neanderthal and *Homo sapiens* means by group. Colors mapped to the Neanderthal mean depict vertices that extend beyond (red) and into (blue) the mesh, relative to Upper Paleolithic hunter-gatherer (a), Holocene hunter-gatherer (b), agriculturalist (c), and postindustrial (d) group means. Per-vertex distance differences are calculated by superimposing the respective group means onto the Neanderthal mean. For instance, the red color of the talar head indicates that the *H. sapiens* head extends beyond the Neanderthal head, resulting in the short neck of the latter. Tali are shown in dorsal (top left), plantar (top right), distal (bottom left), and medial (bottom right) views, respectively. (For interpretation of the references to color in this figure legend, the reader is referred to the Web version of this article.)

the medial column of the foot (Prang, 2016; Sorrentino et al., 2020a) issuing from a more pronated foot in Neanderthals (Sánchez-Rodríguez et al., 2012; Prang, 2016).

The shapes of Neanderthal subtalar articular surfaces are suggestive of a pronated foot posture. Neanderthals appear derived in having distinct posterior and anterior-medial calcaneal facet shapes

that uniquely diverge from both the *H. sapiens* groups and Clark Howell talus (Figs. 2 and 3). In Neanderthals the posterior calcaneal facet is expanded and laterally flattened (Figs. 2c, d and 5), whereas the anterior and middle calcaneal facets appear as a single, relatively round facet (Fig. 3c, d and SOM Fig. S6). Additionally, Neanderthal calcanei have broader articular subtalar surfaces and
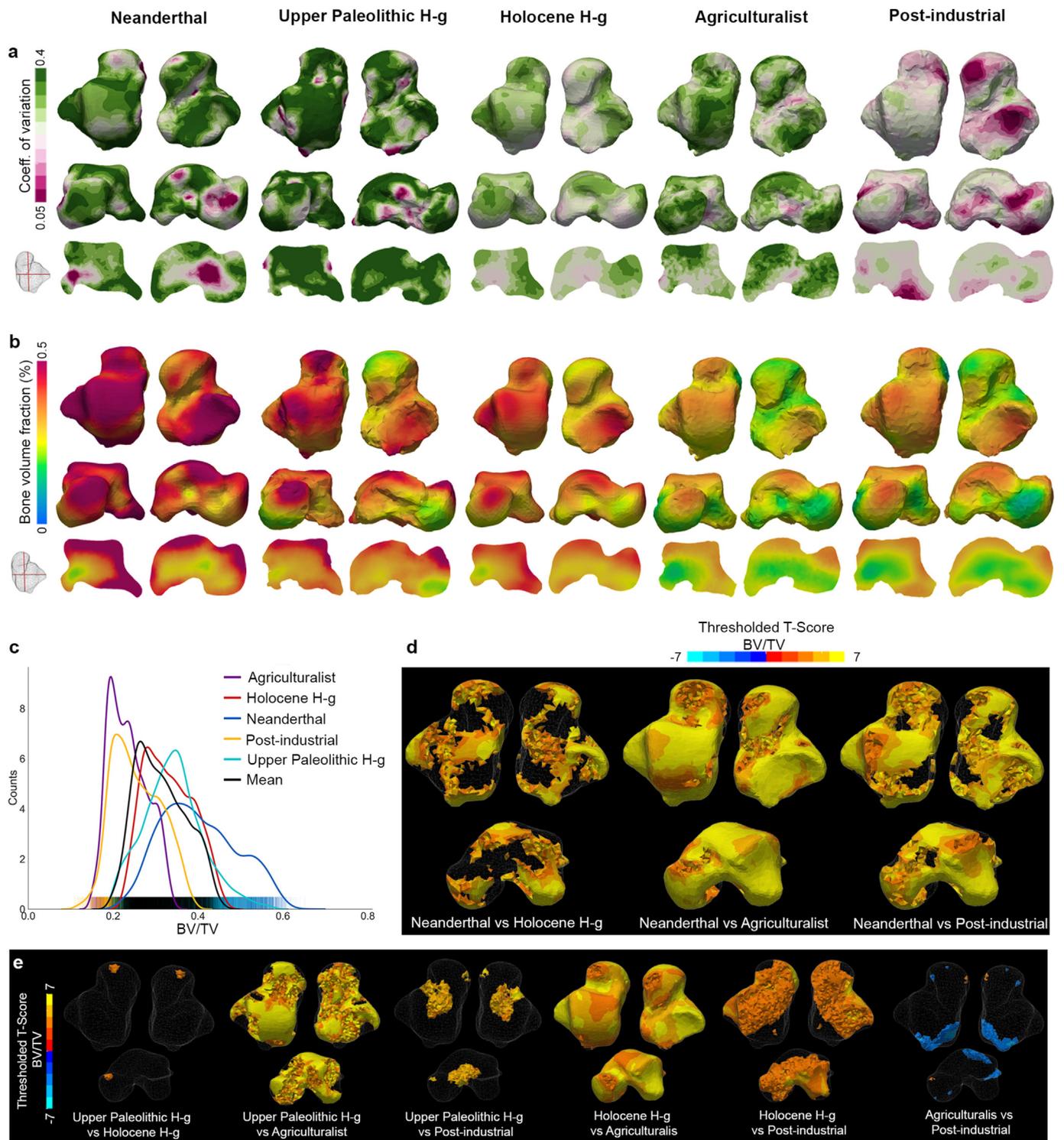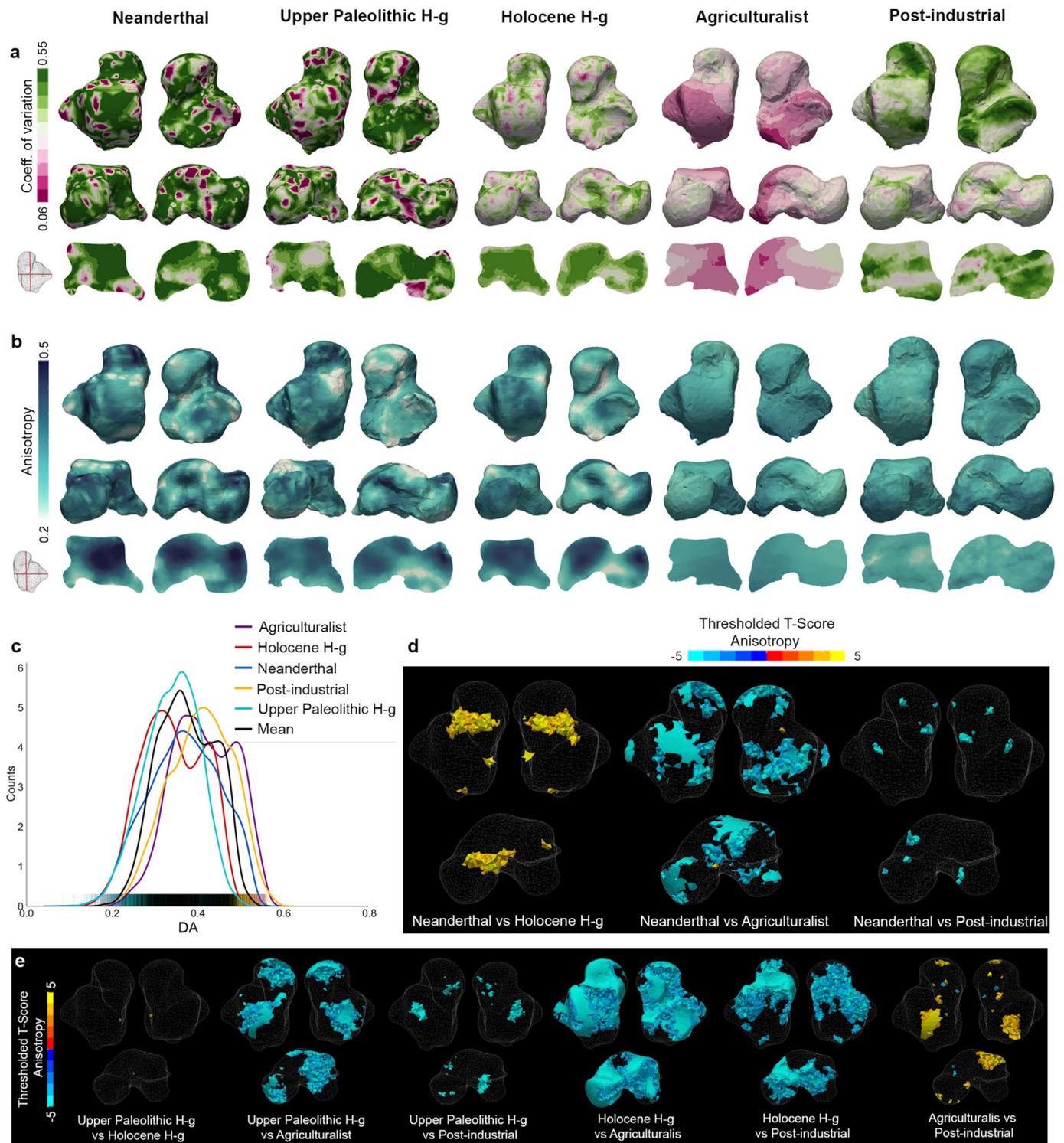
Figure 6. Full bone trabecular differences for BV/TV. Comparison of the site-specific coefficient of variation (a) and BV/TV (b) for the mean of Neanderthal, Upper Paleolithic hunter-gatherer, Holocene hunter-gatherer, agriculturalist, and postindustrial groups. Kernel density distributions representing the counts for each point in the group point clouds are illustrated (c) next to mapped T-scores of significant two-tailed t-tests (d, e). Pairwise results for Neanderthals versus *Homo sapiens* groups are shown along the second row from the bottom (d), with comparisons between *H. sapiens* groups along the bottom row (e). Warm colors indicate where values for the first labeled group are higher than those of the second labeled group (e.g., Neanderthal in Neanderthal vs Holocene hunter-gatherer), while cool colors represent values that are lower in the first labeled group. Abbreviation: H-g = hunter-gatherers. Result of pairwise *t*-score including Neanderthals (*n* = 3) and Upper Paleolithic Hunter-gatherers (*n* = 2) should be interpreted with caution due to the small sample size. (For interpretation of the references to color in this figure legend, the reader is referred to the Web version of this article.)

sustentacula, which are features associated with higher biomechanical stress (Rhoads and Trinkaus, 1977; Trinkaus, 1983).

Morphological variation of both tali and calcanei are expected to, at least, contribute to the kinematics and posture of the foot (Imhauser et al., 2008; Kleipool and Blankevoort, 2010; Button et al., 2015; Tümer et al., 2019). Morphology of the subtalar joint, allowing mainly for eversion and inversion, has been associated with ankle instability when exhibiting less congruent articulating

Figure 7. Full bone trabecular differences for DA. Comparison of the site-specific coefficient of variation (a) and DA (b) for the mean of Neanderthal, Upper Paleolithic hunter-gatherer, Holocene hunter-gatherer, agriculturalist, and postindustrial groups. Kernel density distributions representing the counts for each point in the group point clouds are illustrated (c) next to mapped *t*-scores of significant two-tailed *t*-tests (d, e). Pairwise results for Neanderthals versus *Homo sapiens* groups are shown along the second row from bottom (d), with comparisons between *H. sapiens* groups along the bottom row (e). Warm colors indicate where values for the first labeled group are higher than those of the second labeled group (e.g., Neanderthal in Neanderthal vs Holocene hunter-gatherer), while cool colors represent values that are lower in the first labeled group. Abbreviation: H-g = hunter-gatherers. Result of pairwise *t*-score including Neanderthals (*n* = 3) and Upper Paleolithic Hunter-gatherers (*n* = 2) should be interpreted with caution due to the small sample size. (For interpretation of the references to color in this figure legend, the reader is referred to the Web version of this article.)

surfaces between the talus and calcaneus and a generally flatter joint surface (Tümer et al., 2019). The peculiar subtalar configuration of Neanderthals may suggest less congruent contact between the talus and calcaneus during subtalar motion. Indeed, the fusion of anterior and middle calcaneal facets is reported to be less stable than a separate anterior and middle facet configuration (Bruckner, 1987). An expanded and laterally flattened posterior calcaneal facet reflects increased loading on its lateral side, whereby when the foot
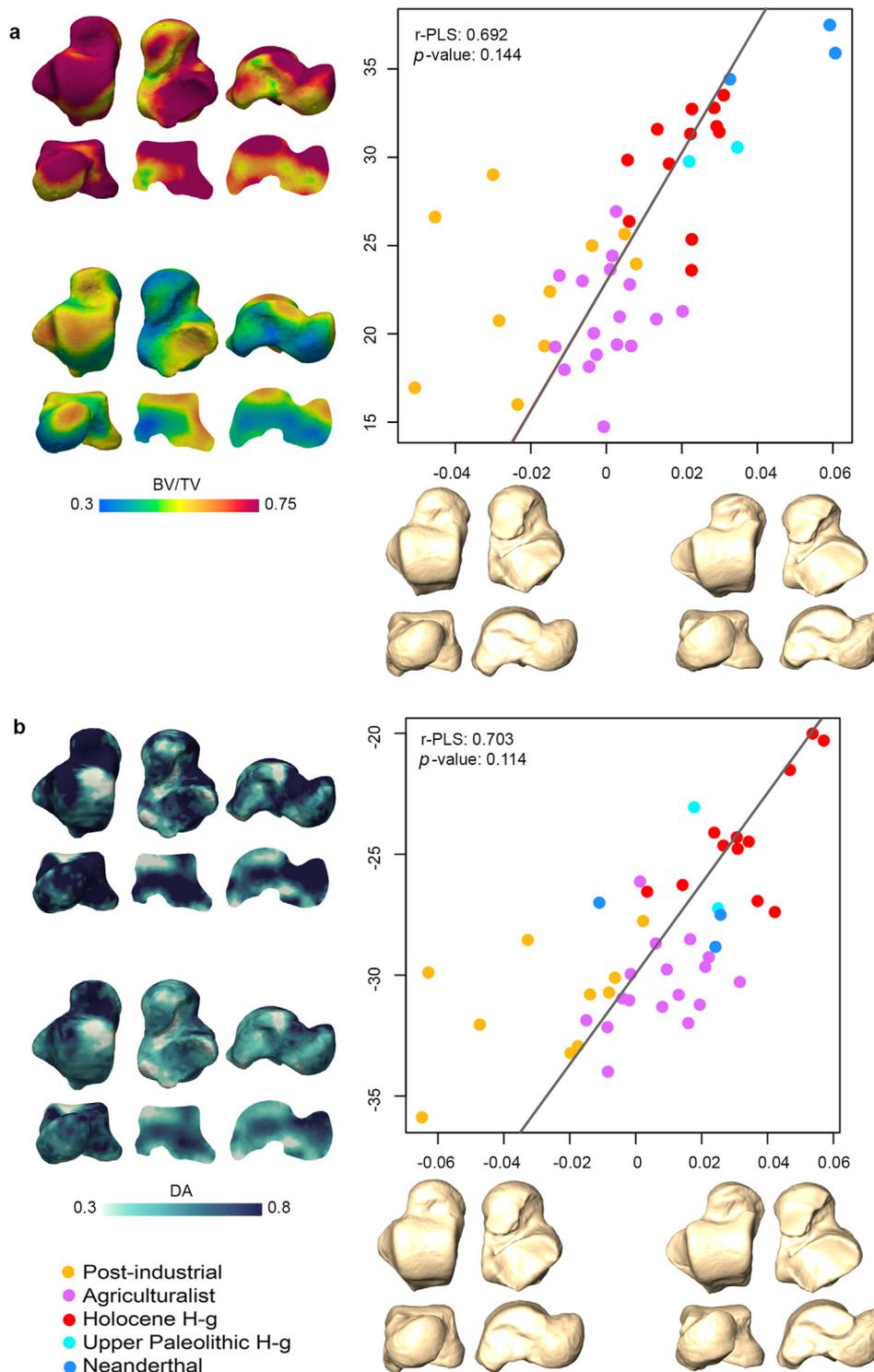
Figure 8. Partial least squares regression of landmark coordinates and trabecular bone point clouds. Covariation of geometric morphometric (semi)landmarks and either BV/TV (a) or DA (b) are determined by the r-coefficient. Abbreviation: H-g = hunter-gatherers.

is everted increased loads will broaden the contact area of the posterior calcaneal facet, while the anterior-medial calcaneal contact area is less affected by the position of the foot (Wagner et al., 1992).

Thus, considering the strong dependency of foot posture and motion on joint morphology, the derived Neanderthal subtalar joint may reflect a tendency for a habitually pronated foot posture

that increased subtalar instability and lateral loading (Fig. 9). Controlled experimental or clinical assessment of the relationship between subtalar joint morphology and foot posture in modern populations can improve our ability to interpret foot posture from pedal fossils. However, this scenario is consistent with the high BV/TV and DA observed throughout the lateral side of the talus (Figs. 6b and 7b), which would act to transmit ground reaction forces from
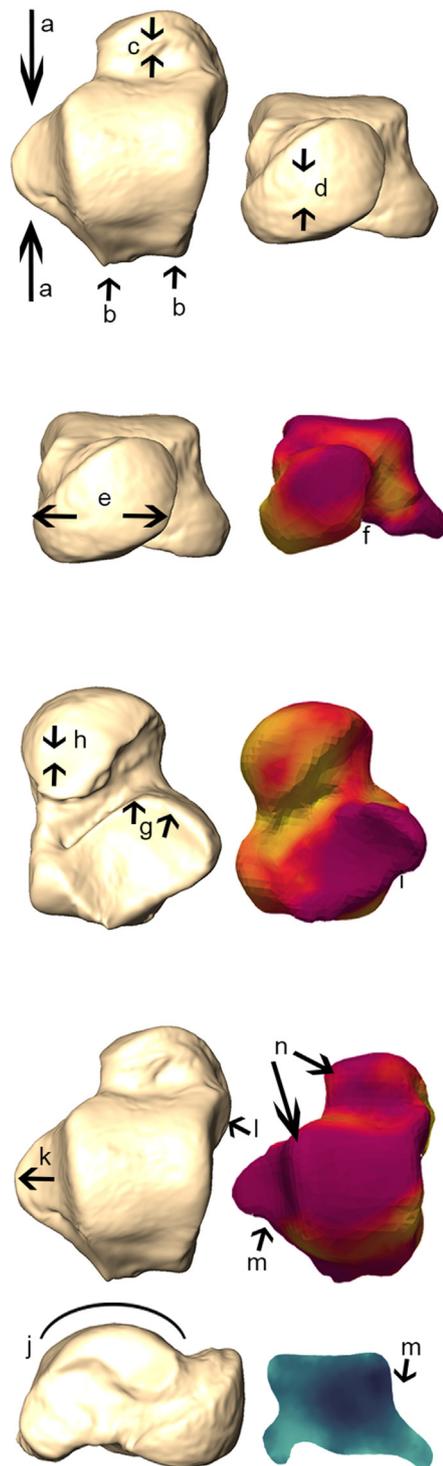
Neanderthal plesiomorphic traits

Overall short talus (a), more rectangular trochlea, less inferiorly and posteriorly projecting medial and lateral tubercles (b), short head and neck (c), dorso-plantarly narrow navicular facet (d), resembling Middle/early Late Pleistocene hominin tali.

Neanderthal mixed plesiomorphic and functional traits

Absolutely medio-laterally broader head and neck (e) with high BV/TV distribution throughout the head and neck (f), resembling the tali of unshod and highly mobile hunter-gatherer *H. sapiens* and Middle/early Late Pleistocene hominins.

Neanderthal autapomorphic traits

Expanded and laterally flattened posterior calcaneal facet (g), and joined, less posteriorly expanded, anterior-medial calcaneal facets (h). Lateral distribution of high BV/TV (i) throughout the posterior calcaneal facet, accounting presumably for a habitually pronated foot posture.

Neanderthal functional traits

Increased dorsal convexity of the trochlea (j), more flared lateral (k) and more cupped medial (l) malleolar facets, higher BV/TV and DA distribution along the superior aspect of the lateral malleolar facet (m), higher BV/TV along the trochlea, and the antero-superior aspect of the head and neck (n). These features are shared with unshod and highly mobile hunter-gatherer *H. sapiens.*

Figure 9. Neanderthal talar traits and description of the main results of this study. The arrows indicate the talar morphological variations expressed in Neanderthals compared with modern human tali.

the calcaneus into relatively broad fibular joint surfaces (Marchi, 2015). Therefore, rather than a supinated posture during stance (Rosas et al., 2017), this suggests a pronated posture during stance, as has been suggested from their highly flared lateral malleolar facet (Pablos et al., 2017). If Neanderthals utilized a pronated foot, they may have experienced ankle instability and injuries consistent with what has been observed in modern humans who exhibit a pronated foot. Modern humans who experience ankle injuries for

excessive foot eversion may develop exostoses and ankle fractures, especially in the fibular malleolus, and deltoid ligament tear (Potter et al., 2012; Stufkens et al., 2012). This may explain the exostoses around articulations and tendon attachments on the distal tibia and fibula of Shanidar 1, the bony spurs in the tibiofibular and talo-fibular attachment sites on the right distal fibula of Shanidar 3, and possibly the degenerative joint disease in Shanidar 1 (trochlea of right talus), Shanidar 3 (sulcus tali, trochlea and subtalar facets of

right talus, and posterior talar surface of the right calcaneus), and Shanidar 5 (posterior calcaneal, medial and lateral malleolar facets), as well as the ligamentous ossifications in the sulcus tali of the left talus of Kiik-Koba 1 (Berger and Trinkaus, 1995; Trinkaus et al., 2008; Trinkaus, 2014; Pomeroy et al., 2017).

Causes of predisposition for a hypothesized pronated foot among Neanderthals are uncertain and need to be further investigated. However, clinical studies have shown prevalence of a pronated foot in obese individuals (Golightly et al., 2014; Butterworth et al., 2015) and also in athletes (e.g., badminton, basketball and volleyball players, and half-marathon runners) who overuse their ankles placing much more force on the foot exceeding their body weight, causing decreased tension in ligaments and increased joint laxity (Kannus, 1992; Cowley and Marsden, 2013; Kuo and Liu, 2017). Thus, it is possible that the greater body mass in Neanderthals could be a genetic contributing factor that elicits this plastic response and secondary expressions of the muscular mass of Neanderthals. Alternatively or concurrently, the more pronated foot in Neanderthals could be a result of plastic features, such as musculoskeletal adaptations for different, high mechanical stress and movement on their ankle. Future studies are needed to elucidate the contributions of these factors to this hypothesized condition in Neanderthals.

Concerning shared morphofunctional traits, the Neanderthal talocrural joint, talar neck, and head resemble more mobile hunter-gatherer *H. sapiens* groups (Figs. 1, 4, 5, and 9; SOM Figs. S3–S5). Similarities in the trochlea among these groups include increased dorsal convexity that would allow for a broader range of dorsal and plantar flexion (Latimer et al., 1987). Higher trochlear convexity in Neanderthals (SOM Fig. S6) may indicate more frequent habitual dorsiflexion, which is in line with the high frequency of a 'squatting facet' observed on the talar neck (Trinkaus, 1975). While the broad talocrural articular surface in their tali is thought to be an adaptation to high levels of activity and biomechanical stress (Rhoads and Trinkaus, 1977), others have suggested that trochlear hypertrophy (i.e., increased overall dimension and medial and anterior extension of trochlea) results from higher body mass (Rosas et al., 2017). Similarly, high body mass has been used to explain the expansion and projection of the lateral malleolar region (Rosas et al., 2017), while others view it as indicating an increased need for talocrural stabilization against laterally directed forces through the ankle or medial weight distribution of the talus (Pablos et al., 2017). The latter would be consistent with higher relative BV/TV and DA distribution along the superior aspect of the medial and lateral malleolar regions (Figs. 6 and 7). This is further supported by the fact that the external and internal morphologies are similar among the highly mobile groups (i.e., Neanderthals and both Upper Paleolithic and Holocene hunter-gatherers; Fig. 8), where results showed no allometric effect for the trochlea or medial and lateral malleolar facets (Table 2). Indeed, a recent study on modern human talar variation found that lateral displacement of the lateral malleolar facet, increased medial malleolar facet cupping, and an anteriorly extended trochlear medial margin are associated with a more everted posture, suggesting more mediolateral stability in a dorsiflexed ankle (Sorrentino et al., 2020b). Although encouraging, further studies on foot posture are needed to help understand why the more mobile groups (e.g., Neanderthals and both Upper Paleolithic and Holocene hunter-gatherers) in this study possess a narrower talocrural articular surface than the Clark Howell (Fig. S6) and Sima de los Huesos tali (Pablos, 2015; Pablos et al., 2017).

More generally, while it could be argued that the lower BV/TV in the agriculturalist and postindustrial groups (Fig. 6) reflects a general shift toward a more gracile skeleton (Chirchir et al., 2015; Ryan and Shaw, 2015), this pattern may also result from lower locomotor demands and the adoption of increasingly sophisticated foot coverings. Among habitually shod populations, transmission of body weight along the medial side of the foot is reduced in magnitude by the use of footwear, limiting strain on the hallux during toe-off (Trinkaus, 2005; Zipfel and Berger, 2007; Mei et al., 2020; Sorrentino et al., 2020b). As such, the broader talar head and neck in presumably unshod hunter-gatherer groups (including Neanderthals) are likely robusticity markers of increased transmission of body weight through the medial column during toe-off (D'Août et al., 2009; Fig.1; SOM Fig. S6), whereas the comparatively more medially displaced talar head and neck may indicate a greater medial deviation of the first metatarsal, as has been observed in modern barefoot hunter-gatherers (Hoffmann, 1905; Barnett, 1962; Zipfel and Berger, 2007; D'Août et al., 2009). Additionally, variations in trabecular patterns of the analyzed groups show lower site-specific BV/TV of more sedentary groups, supporting the idea that there was a reduced need to transmit large loads through the talus (Saers et al., 2018). In contrast, the site-specific BV/TV maps of hunter-gatherers show expanded regions along the lateral aspect of the talus (trochlea, lateral malleolar, and posterior calcaneal facets; Su and Carlson, 2017) and the antero-superior aspect of the head and neck (Tsegai et al., 2017), which overlap with distinct external morphologies. The pattern of variation in DA is less consistent among groups and throughout the regions of the talus. Generally, the relatively high peaks of DA values in the more mobile groups suggests that the most intense loading during locomotion may have been more stereotyped (i.e., higher magnitude and more selectively oriented) than in groups with lower levels of mobility. However, comparisons between *H. sapiens* groups indicate that more mobile groups present also lower peaks of DA values in some regions of the talus than in less mobile groups (e.g., compare Holocene hunter-gatherers vs agriculturalist and postindustrial groups; Fig. 7e), suggesting high levels of variation in joint loading directions of the Holocene hunter-gatherers. Overall, these features are in line with adaptations to the high mobility requirements of a hunting and gathering subsistence strategy, where walking and running along uneven terrain were performed either unshod or wearing minimalistic foot coverings (Carlson et al., 2007; Willems et al., 2017, 2021; Sorrentino et al., 2020b; Table 2; SOM Tables S1 and S2).

Following from this, our results suggest that footwear, subsistence, and mobility have an impact on the talocrural joint, talar neck, and head, which may then be used as distinguishing characteristics between mobility levels (Fig. 9). However, we recognize that the small sample size used to explore aspects of this study acts as a limitation in some ways, and thus, some caution is warranted in the assessment of interactions between the individual variables assessed here (i.e., subsistence, mobility, and footwear) until they are investigated further with larger samples. Furthermore, although the sample composition does not allow us to directly test the effect of ancestry, it is likely that group membership encompasses a combination of variable effects, including ancestry. The Holocene hunter-gatherer and agricultural populations are North American in origin, and they share similar talar morphology and size (Table 3 and SOM Table S5). However, these similarities between the two North American groups may be also indicative of shared levels of locomotor activities or reflecting adaptation to similar geographical territory. Similarly, the Upper Paleolithic hunter-gatherer and postindustrial populations are European (Italian), sharing similar talar size (SOM Table S5), but not overall talar morphology, or trochlear and lateral malleolar shapes (Table 3). Therefore, overall talar variation, or at least some regions of the talus, may reflect genetic affinity among populations along with subsistence, mobility, and footwear use (Turley et al., 2015; Sorrentino, 2020b).

In conclusion, we suggest that the talocrural joint is a functionally and posturally constrained region in both Neanderthals

and *H. sapiens*, whereas the Neanderthal subtalar joint uniquely exhibits autapomorphic features consistent with a habitually pronated foot posture. Furthermore, our results support the view that the navicular facet displays a mixture of ancestral and plastic features reflecting variability in footwear technology and mobility strategies (Fig. 9). Finally, while we found no statistical associations between external and internal features, we suggest that a thorough quantification of both offers complementary insights in interpreting complex morphological relationships and hope that future studies incorporate this dual approach to further our understanding of the morphofunctional differences between Neanderthals and ourselves.

Author contributions

R.S., N.B.S., M.G.B., and S.B. conceived and designed the study. R.S., N.B.S., L.J.D.D., C.F., E.B., F.Ba., J.P.P.S., M.B., F.Bo., G.C., F.F., T.G., H.M., M.P.M., W.P., S.R., and A.R. collected the sample and/or data used in the analyses. R.S. and S.B. carried out the geometric morphometric analysis, and N.B.S. and R.S. performed the trabecular analysis. R.S. and N.B.S. drafted the manuscript. R.S., N.B.S., M.G.B., D.M., T.M.R, J.T.S., K.J.C., and S.B. discussed the results and wrote and edited the manuscript with input from all authors.

Acknowledgments

Supplementary Online Material

Supplementary online material to this article can be found online at https://doi.org/10.1016/j.jhevol.2021.103093.

References

Adams, D.C., Collyer, M.L., 2016. On the comparison of the strength of morphological integration across morphometric datasets. Evolution 70, 2623–2631.

Adams, D.C., Collyer, M.L., 2019. Comparing the strength of modular signal, and evaluating alternative modular hypotheses, using covariance ratio effect sizes with morphometric data. Evolution 73, 2352–2367.

Adams, D., Collyer, M.L., Kaliontzopoulou, A., 2020. Geomorph: Software for geometric morphometric analyses. R package version 3.2.1. Available online: https://cran.r-project.org/package=geomorph.

Aiello, L., Dean, C., 1990. An Introduction to Human Evolutionary Anatomy. Academic Press, London.

Albertin, F., Bettuzzi, M., Brancaccio, R., Morigi, M.P., Casali, F., 2019. X-ray computed tomography *in situ*: An opportunity for museums and restoration laboratories. Heritage 2, 2028–2038.

Ayachit, U., 2015. The ParaView guide: Updated for ParaView version 4.3. Kitware. https://docs.paraview.org/en/latest/.

Barnett, C.H., 1962. The normal orientation of the human hallux and the effect of footwear. J. Anat. 96, 489.

Baxter, J.R., Novack, T.A., Werkhoven, H. Van, Pennell, D.R., Piazza, S.J., 2012. Ankle joint mechanics and foot proportions differ between human sprinters and non-sprinters. Proc. R. Soc. B 279, 2018–2024.

Belcastro, M.G., Bonfiglioli, B., Pedrosi, M.E., Zuppello, M., Tanganelli, V., Mariotti, V., 2017. The History and composition of the identified human skeletal collection of the Certosa cemetery (Bologna, Italy, 19th–20th century). Int. J. Osteoarchaeol. 27, 912–925.

Belcastro, M.G., Mariotti, V., Pietrobelli, A., Sorrentino, R., García-Tabernero, A., Estalrrich, A., Rosas, A., 2020. The study of the lower limb entheses in the Neanderthal sample from El Sidrón (Asturias, Spain): How much musculoskeletal variability did Neanderthals accumulate? J. Hum. Evol. 141, 102746.

Benazzi, S., Nguyen, H.N., Kullmer, O., Hublin, J.J., 2015. Exploring the biomechanics of taurodontism. J. Anat. 226, 180–188.

Benjamini, Y., Hochberg, Y., 1995. Controlling the false discovery rate: A practical and powerful approach to multiple testing. J. R. Stat. Soc. B 57, 289–300.

Berger, T.D., Trinkaus, E., 1995. Patterns of trauma among the Neandertals. J. Archaeol. Sci. 22, 841–852.

Bookstein, F.L., 1991. Morphometric Tools for Landmark Data: Geometry and Biology. Cambridge University Press, Cambridge.

Boyer, D.M., Puente, J., Gladman, J.T., Glynn, C., Mukherjee, S., Yapuncich, G.S., Daubechies, I., 2015. A new fully automated approach for aligning and comparing shapes. Anat. Rec. 298, 249–276.

Boyle, E., DeSilva, J.M., 2015. A large *Homo erectus* talus from Koobi Fora, Kenya (KNM-ER 5428), and Pleistocene hominin talar evolution. PaleoAnthropology 2015, 1–11.

Brietburg, E., 1980. Vertebrate remains from 11SA87a. Center for Archaeological Investigations, Southern Illinois University, Carbondale.

Bruckner, J., 1987. Variations in the human subtalar joint. J. Orthop. Sports Phys. Ther. 8, 489–494.

Brzobohatá, H., Prokop, J., Horák, M., Jančárek, A., Velemínská, J., 2012. Accuracy and benefits of 3D bone surface modelling: A comparison of two methods of surface data acquisition reconstructed by laser scanning and computed tomography outputs. Coll. Antropol. 36, 801–806.

Butterworth, P.A., Urquhart, D.M., Landorf, K.B., Wluka, A.E., Cicuttini, F.M., Menz, H.B., 2015. Foot posture, range of motion and plantar pressure characteristics in obese and non-obese individuals. Gait Posture 41, 465–469.

Carlson, K.J., Marchi, D., 2014. Reconstructing Mobility: Environmental, Behavioral, and Morphological Determinants. Springer, New York.

Carlson, K.J., Grine, F.E., Pearson, O.M., 2007. Robusticity and sexual dimorphism in the postcranium of modern hunter-gatherers from Australia. Am. J. Phys. Anthropol. 134, 9–23.

Chirchir, H., Kivell, T.L., Ruff, C.B., Hublin, J., Carlson, K.J., Zipfel, B., 2015. Recent origin of low trabecular bone density in modern humans. Proc. Natl. Acad. Sci. USA 112, 366–371.

Collyer, M.L., Adams, D.C., 2018. RRPP: An r package for fitting linear models to high-dimensional data using residual randomization. Methods Ecol. Evol. 9, 1772–1779.

Collyer, M.L., Sekora, D.J., Adams, D.C., 2015. A method for analysis of phenotypic change for phenotypes described by high-dimensional data. Heredity 115, 357–365.

Condemi, S., Capecchi, G., Monti, L., Voisin, J.-L., Mounier, A., Ricci, S., Ronchitelli, A., 2014. I resti umani rinvenuti a Paglicci (Rignano Garganico-FG): Nota preliminare. Annali dell'Universita'di Ferrara-Museologia Scientifica e Naturalistica 10, 2.

Cowley, E., Marsden, J., 2013. The effects of prolonged running on foot posture: A repeated measures study of half marathon runners using the foot posture index and navicular height. J. Foot Ankle Res. 6, 1–7.

Craig, O.E., Biazzo, M., Colonese, A.C., Di Giuseppe, Z., Martinez-Labarga, C., Lo Vetro, D., Lelli, R., Martini, F., Rickards, O., 2010. Stable isotope analysis of Late Upper Paleolithic human and faunal remains from Grotta del Romito (Cosenza), Italy. J. Archaeol. Sci. 37, 2504–2512.

D'Août, K., Pataky, T.C., De Clercq, D., Aerts, P., 2009. The effects of habitual footwear use: Foot shape and function in native barefoot walkers. Footwear Sci. 1, 81–94.

DeMars, L.J.D., Stephens, N.B., Saers, J.P.P., Gordon, A., Stock, J.T., Ryan, T.M., 2020. Using point clouds to investigate the relationship between trabecular bone phenotype and behavior: An example utilizing the human calcaneus. Am. J. Hum. Biol. 33, e23468.

DeSilva, J., McNutt, E., Benoit, J., Zipfel, B., 2019. One small step: A review of Plio-Pleistocene hominin foot evolution. Am. J. Phys. Anthropol. 168, 63–140.

di Cesnola, A.P., 2003. Variazioni nel tempo e nello spazio dei riti funerari del Paleolitico superiore italiano. Bull. Paletnol. Ital. 93, 1–17.

Dunmore, C.J., Wollny, G., Skinner, M.M., 2018. MIA-clustering: A novel method for segmentation of paleontological material. PeerJ 6, e4374.

Imhauser, C.W., Siegler, S., Udupa, J.K., Toy, J., 2008. Subject-specific models reveal the existence of a relationship between morphology of the ankle joint complex and its passive mechanical properties. J. Biomech. 41, 1341.

Faith, J.T., 2008. Eland, buffalo, and wild pigs: Were Middle Stone Age humans ineffective hunters? J. Hum. Evol. 55, 24–36.

Fernández, P.J., Mongle, C.S., Leakey, L., Proctor, D.J., Orr, C.M., Patel, B.A., 2018. Evolution and function of the hominin forefoot. Proc. Natl. Acad. Sci. USA 115, 8746–8751.

García-Martínez, D., Torres-Tamayo, N., Torres-Sánchez, I., García-Río, F., Rosas, A., Bastir, M., 2018. Ribcage measurements indicate greater lung capacity in Neanderthals and Lower Pleistocene hominins compared to modern humans. Commun. Biol. 1, 1–9.

Geib, P.R., 2000. Sandal types and archaic prehistory on the Colorado plateau. Am. Antiq. 65, 509–524.

Giacobini, G., 2006. Les sépultures du Paléolithique supérieur: la documentation italienne. C. R. Palevol 5, 169–176.

Golightly, Y.M., Hannan, M.T., Dufour, A.B., Hillstrom, H.J., Jordan, J.M., 2014. Foot disorders associated with overpronated and oversupinated foot function: The johnston county osteoarthritis project. Foot Ankle Int. 35, 1159–1165.

Griffin, N.L., Miller, C.E., Schmitt, D., Ao, K.D., 2015. Understanding the evolution of the windlass mechanism of the human foot from comparative anatomy: Insights, obstacles, and future directions. Am. J. Phys. Anthropol. 156, 1–10.

Gross, T., Kivell, T.L., Skinner, M.M., Nguyen, N.H., Pahr, D.H., 2014. A CT-image-based framework for the holistic analysis of cortical and trabecular bone morphology. Palaeontol. Electron. 17, 1–13.

Grün, R., Stringer, C.B., 1991. Electron spin resonance dating and the evolution of modern humans. Archaeometry 33, 153–199.

Grün, R., Stringer, C., 2000. Tabun revisited: Revised ESR chronology and new ESR and U-series analyses of dental material from Tabun C1. J. Hum. Evol. 39, 601–612.

Guérin, G., Frouin, M., Talamo, S., Aldeias, V., Bruxelles, L., Chiotti, L., Dibble, H.L., Goldberg, P., Hublin, J.-J., Jain, M., Lahaye, C., Madelaine, S., Maureille, B., McPherron, S.J.P., Mercier, N., Murray, A.S., Sandgathe, D., Steele, T.E., Thomsen, K.J., Turq, A., 2015. A multi-method luminescence dating of the Palaeolithic sequence of La Ferrassie based on new excavations adjacent to the La Ferrassie 1 and 2 skeletons. J. Archaeol. Sci. 58, 147–166.

Gunz, P., Mitteroecker, P., 2013. Semilandmarks: A method for quantifying curves and surfaces. Hystrix 24, 103–109.

Harcourt-Smith, W.E.H., 2004. Fossils, feet and the evolution of human bipedal locomotion. J. Anat. 204, 403–416.

Harvati, K., 2010. Neanderthals. Evolution: Education and Outreach 3, 367–376.

Hoffmann, P., 1905. Conclusions drawn from a comparative study of the feet of barefooted and shoe-wearing peoples. J. Bone Jt. Surg. 2, 105–136.

Holowka, N.B., Lieberman, D.E., 2018. Rethinking the evolution of the human foot: Insights from experimental research. J. Exp. Biol. 221, jeb174425.

Holowka, N.B., O'Neill, M.C., Thompson, N.E., Demes, B., 2017. Chimpanzee and human midfoot motion during bipedal walking and the evolution of the longitudinal arch of the foot. J. Hum. Evol. 104, 23–31.

Holowka, N.B., Wallace, I.J., Lieberman, D.E., 2018. Foot strength and stiffness are related to footwear use in a comparison of minimally- vs. conventionally-shod populations. Sci. Rep. 8, 3679.

Holt, B.M., 2003. Mobility in Upper Paleolithic and Mesolithic Europe: Evidence from the lower limb. Am. J. Phys. Anthropol. 122, 200–215.

Holt, B.M., Formicola, V., 2008. Hunters of the Ice Age: The biology of Upper Paleolithic people. Am. J. Phys. Anthropol. 137, 70–99.

Huson, A., 1991. Functional anatomy of the foot. Disorders of the Foot and Ankle 1, 409–431.

Jefferies, R.W., 2013. The archaeology of Carrier Mills: 10,000 years. In: The Saline Valley of Illinois. Southern Illinois University Press, Carbondale.

Kannus, V.P.A., 1992. Evaluation of abnormal biomechanics of the foot and ankle in athletes. Br. J. Sports Med. 26, 83–89.

Kivell, T.L., 2016. A review of trabecular bone functional adaptation: What have we learned from trabecular analyses in extant hominins and what can we apply to fossils? J. Anat. 228, 569–594.

Kleipool, R.P., Blankevoort, L., 2010. The relation between geometry and function of the ankle joint complex: A biomechanical review. Knee Surg. Sports Traumatol. Arthrosc. 18, 618–627.

Kuo, Y.L., Liu, Y.S.F., 2017. The foot posture index between elite athletic and sedentary college students. Kinesiology 49, 202–207.

Latimer, B., Ohman, J.C., Lovejoy, C.O., 1987. Talocrural joint in African hominoids: Implications for *Australopithecus afarensis*. Am. J. Phys. Anthropol. 74, 155–175.

Lieberman, D.E., Devlin, M.J., Pearson, O.M., 2001. Articular area responses to mechanical loading: Effects of exercise, age, and skeletal location. Am. J. Phys. Anthropol. 116, 266–277.

Lockley, M., Roberts, G., Kim, J.Y., 2008. In the footprints of our ancestors: An overview of the hominid track record. Ichnos 15, 106–125.

Lopinot, N., Lynch, M., 1979. An Empirical Examination of Crab Orchard Settlement-Subsistence. Center for Archaeological Investigations, Southern Illinois University, Carbondale.

Lu, Z., Meldrum, D.J., Huang, Y., He, J., Sarmiento, E.E., 2011. The Jinniushan hominin pedal skeleton from the late Middle Pleistocene of China. HOMO 62, 389–401.

Mallegni, F., Bertoldi, F., Manolis, S., 2000. Palaeobiology of two Gravettian skeletons from Veneri cave (Parabita, Puglia, Italy). HOMO 51, 235–257.

Marchi, D., 2010. Articular to diaphyseal proportions of human and great ape metatarsals. Am. J. Phys. Anthropol. 143, 198–207.

Marchi, D., 2015. Using the morphology of the hominoid distal fibula to interpret arboreality in *Australopithecus afarensis*. J. Hum. Evol. 85, 136–148.

Mei, Q., Gu, Y., Xiang, L., Yu, P., Gao, Z., Shim, V., Fernandez, J., 2020. Foot shape and plantar pressure relationships in shod and barefoot populations. Biomech. Model. Mechanobiol. 19, 1211–1224.

Onac, B.P., Viehmann, I., Lundberg, J., Lauritzen, S.E., Stringer, C., Popiță, V., 2005. U–Th ages constraining the Neanderthal footprint at Vârtop Cave, Romania. Quat. Sci. Rev. 24, 1151–1157.

Pablos, A., 2015. The foot in the *Homo* fossil record. Mitteilungen der Gesellschaft für Urgeschichte 24, 1128.

Pablos, A., Pantoja-Pérez, A., Martínez, I., Lorenzo, C., Arsuaga, J.L., 2017. Metric and morphological analysis of the foot in the Middle Pleistocene sample of Sima de los Huesos (Sierra de Atapuerca, Burgos, Spain). Quat. Int. 433, 103–113.

Pablos, A., Gómez-Olivencia, A., Maureille, B., Holliday, T.W., Madelaine, S., Trinkaus, E., Couture-Veschambre, C., 2019. Neandertal foot remains from Regourdou 1 (Montignac-sur-Vézère, Dordogne, France). J. Hum. Evol. 128, 17–44.

Parr, W.C.H., Chatterjee, H.J., Soligo, C., 2011. Inter- and intra-specific scaling of articular surface areas in the hominoid talus. J. Anat. 218, 386–401.

Parr, W.C.H., Soligo, C., Smaers, J., Chatterjee, H.J., Ruto, A., Cornish, L., Wroe, S., 2014. Three-dimensional shape variation of talar surface morphology in hominoid primates. J. Anat. 225, 42–59.

Pearson, O.M., 2000. Activity, climate, and postcranial robusticity. Curr. Anthropol. 41, 569–607.

Pearson, O.M., Cordero, R.M., Busby, A.M., 2006. How different were Neanderthals' habitual activities? A comparative analysis with diverse groups of recent humans. In: Harvati, K., Harrison, T. (Eds.), Neanderthals Revisited: New Approaches and Perspectives. Springer, Dordrecht., pp. 135–156

Pearson, O.M., Royer, D.F., Grine, F.E., Fleagle, J.G., 2008. A description of the Omo I postcranial skeleton, including newly discovered fossils. J. Hum. Evol. 55, 421–437.

Pearson, O.M., Pablos, A., Rak, Y., Hovers, E., 2020. A partial Neandertal foot from the Late Middle Paleolithic of Amud Cave, Israel. PaleoAnthropology 98, 125.

Plavcan, J.M., Meyer, V., Hammond, A.S., Couture, C., Madelaine, S., Holliday, T.W., Maureille, B., Ward, C.V., Trinkaus, E., 2014. The Regourdou 1 Neandertal body size. C. R. Palevol 13, 747–754.

Pomeroy, E., Mirazón Lahr, M., Crivellaro, F., Farr, L., Reynolds, T., Hunt, C.O., Barker, G., 2017. Newly discovered Neanderthal remains from Shanidar Cave, Iraqi Kurdistan, and their attribution to Shanidar 5. J. Hum. Evol. 111, 102–118.

Pomeroy, E., Bennett, P., Hunt, C.O., Reynolds, T., Farr, L., Frouin, M., Holman, J., Lane, R., French, C., Barker, G., 2020. New Neanderthal remains associated with the 'flower burial' at Shanidar Cave. Antiquity 94, 11–26.

Potter, M.Q., Blankenhorn, B.D., Avilucea, F.R., Beals, T.C., Nickisch, F., 2012. Osseous talofibular impingement after supination–external rotation stage II ankle fracture: Case report. Foot Ankle Int. 33, 1006–1010.

Prang, T.C., 2015. Rearfoot posture of *Australopithecus sediba* and the evolution of the hominin longitudinal arch. Sci. Rep. 5, 1–9.

Prang, T.C., 2016. Conarticular congruence of the hominoid subtalar joint complex with implications for joint function in Plio-Pleistocene hominins. Am. J. Phys. Anthropol. 160, 446–457.

R Core Team, 2019. R: A language and environment for statisticalcomputing. R Foundation for Statistical Computing, Vienna, Austria. https://www.R-project.org/.

Rhoads, J.G., Trinkaus, E., 1977. Morphometrics of the Neandertal talus. Am. J. Phys. Anthropol. 46, 29–43.

Rink, W.J., Schwarcz, H.P., Smith, F.H., Radovčić, J., 1995. ESR ages for Krapina hominids. Nature 378, 24.

Rink, W.J., Schwarcz, H.P., Lee, H.K., Rees-Jones, J., Rabinovich, R., Hovers, E., 2001. Electron spin resonance (ESR) and thermal ionization mass spectrometric (TIMS) 230Th/234U dating of teeth in Middle Paleolithic layers at Amud Cave, Israel. Geoarchaeology 16, 701–717.

Rohlf, F.J., Corti, M., 2000. Use of two-block partial least-squares to study covariation in shape. Syst. Biol. 49, 740–753.

Ronchitelli, A., Mugnaini, S., Arrighi, S., Atrei, A., Capecchi, G., Giamello, M., Longo, L., Marchettini, N., Viti, C., Moroni, A., 2015. When technology joins symbolic behaviour: The Gravettian burials at Grotta Paglicci (Rignano Garganico - Foggia - Southern Italy). Quat. Int. 359, 423–441.

Rosas, A., Ferrando, A., Bastir, M., García-Tabernero, A., Estalrrich, A., Huguet, R., García-Martínez, D., Pastor, J.F., de la Rasilla, M., 2017. Neandertal talus bones from El Sidrón site (Asturias, Spain): A 3D geometric morphometrics analysis. Am. J. Phys. Anthropol. 164, 394–415.

Ruff, C.B., Holt, B.M., Niskanen, M., Sladék, V., Berner, M., Garofalo, E., Garvin, H.M., Hora, M., Maijanen, H., Niinimäki, S., Salo, K., Schuplerová, E., Tompkins, D., 2012. Stature and body mass estimation from skeletal remains in the European Holocene. Am. J. Phys. Anthropol. 148, 601–617.

Ryan, T.M., Shaw, C.N., 2015. Gracility of the modern *Homo sapiens* skeleton is the result of decreased biomechanical loading. Proc. Natl. Acad. Sci. USA 112, 372–377.

Saers, J.P.P., Ryan, T.M., Stock, J.T., 2018. Trabecular bone functional adaptation and sexual dimorphism in the human foot. Am. J. Phys. Anthropol. 168, 154–169.

Saers, J.P.P., Ryan, T.M., Stock, J.T., 2019. Trabecular bone structure scales allometrically in the foot of four human groups. J. Hum. Evol. 135, 102654.

Sánchez-Rodríguez, R., Martínez-Nova, A., Escamilla-Martínez, E., Pedrera-Zamorano, J.D., 2012. Can the Foot Posture Index or their individual criteria predict dynamic plantar pressures? Gait Posture 36, 591–595.

Santure, S.K., Harn, A.D., Esarey, D., 1990. Archaeological Investigations at the Morton Village and Norris Farms 36 Cemetery. Illinois State Museum, Springfield.

Schlager, S., 2017. Morpho and Rvcg - Shape Analysis in R: R-Packages for Geometric Morphometrics, Shape Analysis and Surface Manipulations. In: Zheng, G., Ll, S., Székely, G. (Eds.), Statistical Shape and Deformation Analysis: Methods, Implementation and Applications, 1st ed. Academic Press, London, pp. 217–256.

Schneider, C.A., Rasband, W.S., Eliceiri, K.W., 2012. NIH Image to ImageJ: 25 years of image analysis. Nat. Methods 9, 671–675.

Semal, P., Rougier, H., Crevecoeur, I., Jungels, C., Flas, D., Hauzeur, A., Maureille, B., Germonpré, M., Bocherens, H., Pirson, S., Cammaert, L., De Clerck, N., Hambucken, A., Higham, T., Toussaint, M., van der Plicht, J., 2009. New data on the late Neandertals: Direct dating of the Belgian Spy fossils. Am. J. Phys. Anthropol. 138, 421–428.

Shaw, C.N., Stock, J.T., 2013. Extreme mobility in the Late Pleistocene? Comparing limb biomechanics among fossil Homo, varsity athletes and Holocene foragers. J. Hum. Evol. 64, 242–249.

Slice, D.E., 2005. Modern Morphometrics in Physical Anthropology. Kluwer Academic/Plenum Publishers, New York.

Sorrentino, R., Carlson, K.J., Bortolini, E., Minghetti, C., Feletti, F., Fiorenza, L., Frost, S., Jashashvili, T., Parr, W., Shaw, C., Su, A., Turley, K., Wroe, S., Ryan, T.M., Belcastro, M.G., Benazzi, S., 2020a. Morphometric analysis of the hominin talus: Evolutionary and functional implications. J. Hum. Evol. 142, 102747.

Sorrentino, R., Stephens, N.B., Carlson, K.J., Figus, C., Fiorenza, L., Frost, S., Harcourt-Smith, W., Parr, W., Saers, J., Turley, K., Wroe, S., Belcastro, M.G., Ryan, T.M., Benazzi, S., 2020b. The influence of mobility strategy on the modern human talus. Am. J. Phys. Anthropol. 171, 456–469.

Sorrentino, R., Belcastro, M.G., Figus, C., Stephens, N.B., Turley, K., Harcourt-Smith, W., Ryan, T.M., Benazzi, S., 2020c. Exploring sexual dimorphism of the modern human talus through geometric morphometric methods. PLoS One 15, e0229255.

Stephens, N.B., 2020. Phenotypic PointCloud Analysis. Zenodo. https://doi.org/10.5281/zenodo.4006528. Deposited. https://www.github/NBStephens/Phenotypic_PointCloud_Analysis. (Accessed 18 November 2020).

Stephens, N.B., Kivell, T.L., Pahr, D.H., Hublin, J.J., Skinner, M.M., 2018. Trabecular bone patterning across the human hand. J. Hum. Evol. 123, 1–23.

Steudel-Numbers, K.L., Tilkens, M.J., 2004. The effect of lower limb length on the energetic cost of locomotion: Implications for fossil hominins. J. Hum. Evol. 47, 95–109.

Stufkens, S.A., van den Bekerom, M.P., Knupp, M., Hintermann, B., van Dijk, C.N., 2012. The diagnosis and treatment of deltoid ligament lesions in supination–external rotation ankle fractures: A review. Strategies Trauma Limb Reconstr. 7, 73–85.

Su, A., Carlson, K.J., 2017. Comparative analysis of trabecular bone structure and orientation in South African hominin tali. J. Hum. Evol. 106, 1–18.

Theska, T., Sieriebriennikov, B., Wighard, S.S., Werner, M.S., Sommer, R.J., 2020. Geometric morphometrics of microscopic animals as exemplified by model nematodes. Nat. Protoc. 15, 2611–2644.

Tingran, G., Winchester, J., Stephens, N., 2020. Auto3dgm-matlab-gorgon: Auto3dgm with Transformation Matrices. Zenodo. https://doi.org/10.5281/zenodo.4006528. https://Github.com/NBStephens/auto3dgm-matlab-gorgon. (Accessed 18 November 2020). Deposited.

Trinkaus, E., 1975. Squatting among the Neandertals: A problem in the behavioral interpretation of skeletal morphology. J. Archaeol. Sci. 2, 327–351.

Trinkaus, E., 1983. Functional aspects of Neandertal pedal remains. Foot Ankle 3, 377–390.

Trinkaus, E., 2005. Anatomical evidence for the antiquity of human footwear use. J. Archaeol. Sci. 32, 1515–1526.

Trinkaus, E., 2006. Modern human versus Neandertal evolutionary distinctiveness. Curr. Anthropol. 47, 597–620.

Trinkaus, E., 2014. The Shanidar Neandertals. Academic Press.

Trinkaus, E., Churchill, S.E., Villemeur, I., Riley, K.G., Heller, J.A., Ruff, C.B., 1991. Robusticity versus shape: The functional interpretation of Neandertal appendicular morphology. J. Anthropol. Soc. 99, 257–278.

Trinkaus, E., Maley, B., Buzhilova, A.P., 2008. Brief communication: Paleopathology of the Kiik-Koba 1 Neandertal. Am. J. Phys. Anthropol. 137, 106–112.

Tsegai, Z.J., Skinner, M.M., Gee, A.H., Pahr, D.H., Treece, G.M., Hublin, J., Kivell, T.L., 2017. Trabecular and cortical bone structure of the talus and distal tibia in *Pan* and *Homo*. Am. J. Phys. Anthropol. 163, 784–805.

Tümer, N., Vuurberg, G., Blankevoort, L., Kerkhoffs, G.M.M.J., Tuijthof, G.J.M., Zadpoor, A.A., 2019. Typical shape differences in the subtalar joint bones between subjects with chronic ankle instability and controls. J. Orthop. Res. 37, 1892–1902.

Turley, K., White, F.J., Frost, S.R., 2015. Phenotypic plasticity: The impact of habitat and behavior (substrate use) on adult talo-crural appositional articular joint shape both between and within closely related hominoid species. Hum. Evol. 30, 49–67.

Vercellotti, G., Alclati, G., Richards, M.P., Formicola, V., 2008. The Late Upper Paleolithic skeleton Villabruna 1 (Italy): A source of data on biology and behavior of a 14.000 year-old hunter. J. Anthropol. Sci. 86, 143–163.

Wagner, U.A., Sangeorzan, B.J., Harrington, R.M., Tencer, A.F., 1992. Contact characteristics of the subtalar joint: Load distribution between the anterior and posterior facets. J. Orthop. Res. 10, 535–543.

Waltenberger, L., Rebay-Salisbury, K., Mitteroecker, P., 2021. Three-dimensional surface scanning methods in osteology: A topographical and geometric morphometric comparison. Am. J. Phys. Anthropol. 17, 846–858.

Weaver, T.D., 2009. The meaning of Neandertal skeletal morphology. Proc. Natl. Acad. Sci. USA 106, 16028–16033.

Weaver, T.D., Steudel-Numbers, K., 2005. Does climate or mobility explain the differences in body proportions between Neandertals and their Upper Paleolithic successors? Evol. Anthropol. 14, 218–223.

Weaver, T.D., Roseman, C.C., Stringer, C.B., 2007. Were neandertal and modern human cranial differences produced by natural selection or genetic drift? J. Hum. Evol. 53, 135–145.

Willems, C., Stassijns, G., Cornelis, W., D'Août, K., 2017. Biomechanical implications of walking with indigenous footwear. Am. J. Phys. Anthropol. 162, 782–793.

Willems, C., Curtis, R., Pataky, T., D'Août, K., 2021. Plantar pressures in three types of indigenous footwear, commercial minimal shoes, and conventional Western shoes, compared to barefoot walking. Footwear Sci. 13, 1–17.

Worsley, K.J., Marrett, S., Neelin, P., Vandal, A.C., Friston, K.J., Evans, A.C., 1996. A unified statistical approach for determining significant signals in images of cerebral activation. Hum. Brain Mapp. 4, 58–73.

Wroe, S., Parr, W.C.H., Ledogar, J.A., Bourke, J., Evans, S.P., Fiorenza, L., Benazzi, S., Hublin, J.J., Stringer, C., Kullmer, O., Curry, M., Rae, T.C., Yokley, T.R., 2018. Computer simulations show that Neanderthal facial morphology represents adaptation to cold and high energy demands, but not heavy biting. Proc. R. Soc. B 285, 20180085.

Zipfel, B., Berger, L.R., 2007. Shod versus unshod: The emergence of forefoot pathology in modern humans? Foot 17, 205–213.